Applied Thermal Engineering 214 (2022) 118739

Contents lists available at ScienceDirect

Applied Thermal Engineering

journal homepage: www.elsevier.com/locate/apthermeng

Potentials and challenges for pillow-plate heat exchangers: State-of-the-art review

Mahmood Mastani Joybari [a,*], Håkon Selvnes [b], Alexis Sevault [b], Armin Hafner [a]

[a] Department of Energy and Process Engineering, Norwegian University of Science and Technology, Kolbjørn Hejes vei 1D, Trondheim 7491, Norway
[b] SINTEF Energy Research, Postboks 4761 Torgarden, Trondheim 7465, Norway

ARTICLE INFO

Keywords:
Pillow-plates
Heat exchanger
Heat transfer
Thermohydraulic performance
Literature review

ABSTRACT

For a long time, shell-and-tube heat exchangers have been the most common choice in the industry. Despite some limitations, their main advantage is that they have been extensively investigated and reliable design tools are readily available. In other words, any alternative design should not only outperform shell-and-tube heat exchangers, but also be equipped with a comparably reliable and robust design platform for engineers. In recent years, a growing market share can be observed for plate heat exchangers, particularly for a special class known as pillow-plate heat exchangers. Recently, the research on pillow-plate heat exchangers has gained momentum primarily due to their relative low cost, compact design and structural integrity. However, a comprehensive literature review on the advancements so far and challenges ahead of their widespread application is missing. This study aims to fill this gap in the literature by systematically, critically and comprehensively surveying earlier studies on pillow-plate heat exchangers and providing an in-depth discussion regarding the achievements so far. The findings of this study are expected to help direct the forthcoming research on pillow-plate heat exchangers, especially towards more robust design tools. Overall, further investigation is needed on cost, plate material, flow configuration, heat transfer enhancement, correlation development, two-phase flow, etc.

1. Introduction

Heat exchange between two fluids is very common in process industries. Sustainability mandates heat exchanger designers to introduce more compact, energy efficient designs, requiring less material. Besides, structural integrity, withstanding high pressures and hermetically sealed construction are other beneficial assets for heat exchangers. Pillow-plate heat exchangers (PPHXs) meet these requirements and have found application in many industries (e.g., HVAC industry [1], food industry especially for dairy [2], chocolate and wine [3], and pulp and paper industry [4]).

Despite such widespread applications, the literature and (to a greater extent) industry have not been consistent on naming this type of heat exchangers. Aside from PPHXs, they have been referred to as thermoplates, pillow-plates, embossed plate heat exchangers, welded plate heat exchangers, etc. Note that the term "thermoplate" does not necessarily mean a PPHX. Besides, a PPHX normally stands for a stack of several pillow-plates [5], which create two heat transfer fluid (HTF) passages within and between plates [6]. Advantages of PPHXs compared to shell-and-tube heat exchangers (STHXs) are their simple installation and reduced size [7]. Plate heat exchangers (PHXs) are favorable due to their low approach temperature; however, they face cost restrictions [1]. Meanwhile, PPHXs are not only economically manufacturable with more design freedom, but they are also more efficient thermohydraulically. In the HVAC industry, PPHXs benefit from compactness and better temperature approach as well as less material and refrigerant requirements [2]. They have also been utilized as evaporators [8] and gas coolers [9] as well as internal condensers in distillation columns [6]. Nevertheless, compared to other heat exchangers, PPHXs have not been thoroughly investigated and reliable design tools are currently missing.

Fig. 1 shows the number and type of publications on PPHXs per

Abbreviations: CFD, Computational fluid dynamics; CHT, Conjugate heat transfer; CSF, Continuum surface force; CTES, Cold thermal energy storage; DES, Detached eddy simulation; FCE, Forced circulation evaporation; HTF, Heat transfer fluid; HVAC, Heating, ventilation and air conditioning; IC, Inner channel; LES, Large eddy simulation; MC, Meandering core; NCE, Natural circulation evaporation; OC, Outer channel; PCM, Phase change material; PEC, Performance evaluation criterion; PHX, Plate heat exchanger; PPHX, Pillow-plate heat exchanger; RANS, Reynolds-averaged Navier Stokes; RSW, Refrigerated seawater; STHX, Shell-and-tube heat exchanger; VOF, Volume of fluid; WALE, Wall adapting local eddy-viscosity; WHR, Width to height ratio; WS, Weld-spot.

* Corresponding author.
E-mail address: mahmood.m.joybari@ntnu.no (M. Mastani Joybari).

https://doi.org/10.1016/j.applthermaleng.2022.118739
Received 20 February 2022; Received in revised form 23 May 2022; Accepted 25 May 2022
Available online 30 May 2022

Nomenclature

A	Area (m^2)
B	Spacing between the two adjacent pillow plates (m or mm)
Bo	Boiling number (-)
c	Correlation constant (-)
d	Diameter (m)
f	Corrective function (-)
g	Gravitational acceleration (m/s^2)
h	Heat transfer coefficient ($W/m^2.K$)
h_i	Maximum inflation height (m or mm)
h_o	Plate pitch (m or mm)
H	Specific enthalpy (J/kg)
k	Thermal conductivity (W/m.K)
Ka	Kapitza number (-)
L	Total length of the heat exchanger (m)
m	Correlation exponent (-)
$\dot{m}$	Mass flow rate (kg/s)
n	Correlation exponent (-)
N	Number of pillow plates (-)
Nu	Nusselt number (-)
P	Pressure (Pa)
Pr	Prandtl number (-)
q	Vapor quality (-)
$\dot{q}$	Heat flux (W/m^2)
r	Specific thermal resistance ($m^2.K/W$)
Re	Reynolds number (-)
s	Pitch (m or mm)
Sc	Schmidt number (-)
Sh	Sherwood number (-)
T	Temperature (K or °C)
u	Velocity (m/s)
V	Volume (m^3)
$\dot{V}$	Volumetric flow rate (m^3/s)
W	Total width of the heat exchanger (m)
x	Cartesian coordinate
y	Cartesian coordinate
z	Cartesian coordinate

Subscripts

0	Projection, reference
A	Area
$bundle$	Tube bundle
con	Condensation
$corr$	Corrected
CS	Cross-sectional
D	Diagonal
dia	Weld-spot diameter
f	Film
h	Hydraulic
IC	Inner channel
in	Inlet
inf	Inflation height
HT	Heat transfer
liq	Liquid
L	Longitudinal
max	Maximum
MC	Meandering core
OC	Outer channel
out	Outlet
p	Periodic
pcm	Phase change material
R	Reduced
$ratio$	Ratio
T	Transversal
$Temp$	Temperature-dependent
Tot	Total
V	Volumetric
vap	Vapor
W	Wall
ws	Weld-spot
Wet	Wetted

Greek symbols

δ	Plate thickness (m or mm)
ζ	Friction factor (-)
η	Fin efficiency (-)
ε	Thermohydraulic efficiency or effectiveness (-)
ρ	Density (kg/m^3)
μ	Dynamic viscosity (Pa.s)
ν	Kinematic viscosity (m^2/s)
σ	Surface tension (N/m)
ϕ	Dimensionless weld-spot parameter (-)
ψ	Dimensionless parameter (-)
χ	Thermohydraulic efficiency ratio (-)
Δ	Difference
Γ	Specific mass flow rate (kg/m.s)

annum discussed in this study. It clearly indicates that PPHXs have recently received academic attention and consequently more potential for industrial market penetration. The objective of this study is to conduct a comprehensive literature review to present the state-of-the-art on PPHXs, discussing the achievements so far and challenges ahead of their widespread application.

2. Characterization

This section presents the PPHX formation process, design parameters, common materials, possible configurations and some geometrical parameters.

2.1. Formation process

2.1.1. Old technique

The concept of PPHX design can be traced back to early 70s (e.g., [10]). Normally, two identically thick metallic sheets (commonly stainless steel [6]) are superimposed. Thereafter, all the edges except those considered for fluid flow are seam-welded. The structure is then placed inside a pressure vessel equipped with some fixtures. The fixtures keep the plates pressed and are located where the spots are anticipated. Then the plates are hydraulically inflated (known as hydroforming). Finally, the fixture points are spot-welded, forming a uniform geometry.

2.1.2. Current technique

The technique used nowadays was introduced in late 90s (e.g., [11]), in which, once the plates are superimposed, they are first spot-welded (laser/resistance welding [5]) following a pattern (discussed in Section 2.4.2). Thereafter, the edges (except the inlet and outlet) are seam-welded followed by hydroforming. Therefore, the current technique requires no pressure vessel, simplifying the formation process. Moreover, since typical hydroforming pressures are beyond typical operating conditions, PPHXs are considered hermetically-sealed [6].

2.1.3. Possible future technique

Enhanced surfaces outperform smooth ones due to the extended heat transfer area. Nevertheless, the current technique is limited to smooth plates, since surface enhancement significantly increases the stiffness, causing troubles during hydroforming [12]. A possible solution is incremental electrohydraulic forming [13], in which thinner plates can also be used due to incrementally increasing the second moment of inertia [14].

2.2. Design parameters

The PPHX design parameters are (see Fig. 2):

- **Plate thickness (δ):** Its minimum value is dictated by the required structural integrity of the heat exchanger. Thicker plates not only require higher hydroforming pressure but also increase the thermal resistance.
- **Weld-spot diameter (d_{ws}):** It affects the flow both within and between plates by disrupting the boundary layer formation.
- **Longitudinal pitch (s_L)/transversal pitch (s_T):** The pitch ratio plays an important role in flow characteristics (discussed in Section 5.3).
- **Total width (W)/total length (L):** Knowing these parameters so far, the plate can be spot-welded, ready for hydroforming.
- **Maximum inflation height (h_i):** Depending on the parameters so far, hydroforming pressure can reach 7000 kPa [15] to achieve the desired inner channel (IC) inflation.
- **Number of plates (N):** So far, the design parameters for a single pillow-plate have been established which has to be repeated to create N plates.
- **Distance between adjacent plates (h_o):** This step finalizes the PPHX design and creates the outer channel (OC).

Note that the HTF with higher fouling is recommended to flow in OC. The reason is that OC can be cleaned either chemically or mechanically, whereas IC can only be cleaned chemically or with return flow [6]. If fouling is not a concern, the fluid exceeding its allowable pressure drop should flow in OC where by adjusting the plates distance, the allowable pressure drop can be achieved [16]. Typical PPHX dimensions are 300–2000 mm width, 700–8000 mm length (or height) and 8–12 mm WS diameter [6] while in applications with high operating pressure, more WSs per plate area can be used [17]. Table 1 summarizes the investigated studies on PPHXs with their objectives in Table 2.

Note that no convention exists for the definition of the longitudinal and transversal pitches. Fig. 2a and b show the definitions in the older and more recent studies, respectively. It is worth cautioning that some recent studies reported s_L (instead of $2s_L$). Therefore, these definitions can be both ambiguous and troublesome when considering multiple studies. Nevertheless, to avoid further confusion, the latter (i.e., Fig. 2b) was followed in this text.

Moreover, according to Fig. 3, pillow-plate waviness causes a maximum and minimum distance in between plates (i.e., $h_{o,\max}$ and $h_{o,\min}$, respectively), while plate pitch (i.e., spacing) is considered as the middle-to-middle distance between two pillow-plates (similar to center-to-center pitch in STHXs). Some studies did not specify which value was reported while some used them interchangeably. To harmonize this geometric definition in this study, $h_{o,\max}$ was used (hereinafter referred to as h_o).

Aside from the design parameters, some geometrical/dimensionless parameters are used for instance in heat transfer calculations. This section discusses some of these parameters to present the findings of earlier studies.

2.2.1. Periodic and projection areas

Fig. 4a shows the periodic area (A_p), the smallest symmetric plate area (black dashed boundary in Fig. 4b). Projection area (A_0), shown by the solid red boundary in Fig. 4b, is obtained by subtracting the area of WSs (A_{ws}) from the periodic area.

2.2.2. Dimensionless geometrical parameters

Some dimensionless parameters have been defined to characterize the PPHX geometry. Commonly, the design parameters were non-dimensionalized with reference to transversal pitch, e.g., pitch ratio [9]:

$$s_{ratio} = \frac{2s_L}{s_T} \tag{1}$$

Similarly, for WS diameter and maximum inflation height [9]:

$$s_{dia} = \frac{d_{ws}}{s_T} \tag{2}$$

$$s_{inf} = \frac{h_i}{s_T} \tag{3}$$

Dimensionless WS parameter was defined to characterize pillow-

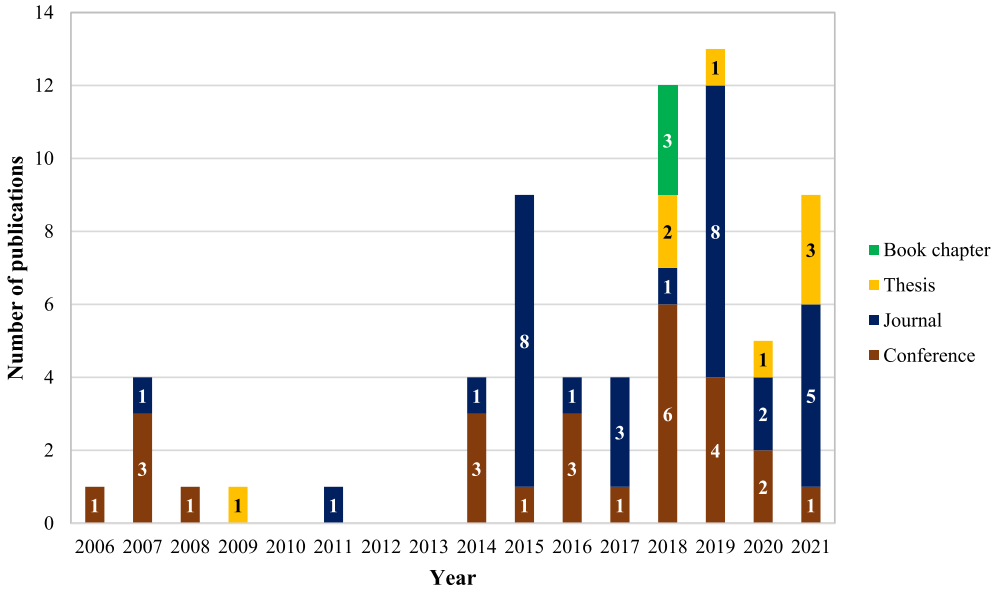

Fig. 1. Number and type of studies conducted on PPHXs per annum discussed in this paper.

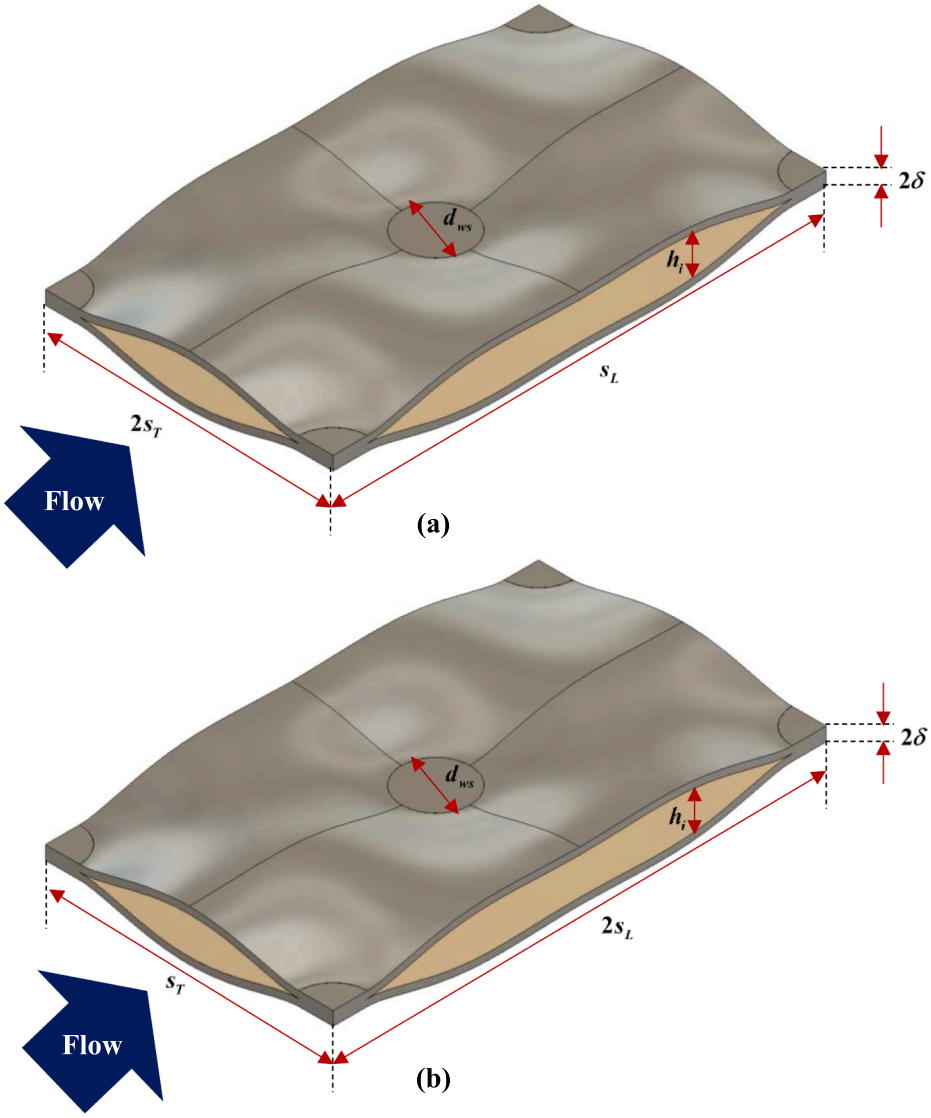

Fig. 2. Design parameters indicating the pitch definitions according to (a) older studies and (b) recent studies.

plates especially for up/downscaling purposes. It indicates what portion of the periodic area is not covered with WSs [18]:

$$\phi_A = \frac{A_0}{A_p} = 1 - \frac{\pi d_{ws}^2}{4 s_L s_T} \tag{4}$$

Another parameter exists to account for the difference between IC and OC areas since the latter is extended by the WSs [4]:

$$\psi_{ws} = \frac{A_{ws}}{A_{IC}} = \frac{A_{OC} - A_{IC}}{A_{IC}} \tag{5}$$

2.2.3. Diagonal and reduced weld-spot pitches

Diagonal WS pitch was defined for up/downscaling purposes and indicates the minimum distance between each pair of neighboring WSs (center-to-center) [18]:

$$s_D = \sqrt{\left(\frac{2s_L}{2}\right)^2 + \left(\frac{s_T}{2}\right)^2} \tag{6}$$

shown in green in Fig. 4b. A similar parameter exists excluding WS diameter [19]:

$$s_{D,ws} = \sqrt{\left(\frac{2s_L - d_{ws}}{2}\right)^2 + \left(\frac{s_T - d_{ws}}{2}\right)^2} \tag{7}$$

Finally, reduced WS pitch was defined similar to the pitch ratio but subtracting WS diameter [20]:

$$s_R = \frac{2s_L - d_{ws}}{s_T - d_{ws}} \tag{8}$$

2.3. Common materials

According to Table 1, aside from one numerical study with pure aluminum [4], different stainless steel (SS) types, especially AISI304 and AISI321, dominated all the studies. However, the thermophysical properties of SS are not suitable for efficient heat transfer, especially its low thermal conductivity. Copper possesses superior thermophysical properties and is widely used in STHXs; however, its spot-welding and hydroforming are not easy. Most probably the old formation technique (see Section 2.1.1) can be used for copper, but few reasons might hinder its application: (1) ease of manufacturing with the new technique (see Section 2.1.2), (2) widespread application of PPHXs in food industry (especially dairy) where SS is required due to sanitary issues and (3)

Table 1
Chronological summary of the literature in terms of investigated design parameters. (See below-mentioned references for further information.)

No.	Year	Reference	Study type[&]	Phase	Inner channel		Outer channel		Material	d_{ws}[mm]	s_T[mm]	$2s_L$[mm]	h_i[mm]	L[mm]	W[mm]	δ[mm]	N[-]	h_o[mm]	Pattern[^]	Flow	Orientation
					Phenomenon	HTF	Phenomenon	HTF													
1	2006	Mitrovic and Maletic [21]	N	Single	Heating	Water	NA	NA	NM	10	72	Varied	Varied	Varied	72	NM	1	NA	NM	NA	NM
2	2007	Mitrovic and Maletic [7]	N	Single	Heating	Water	NA	NA	NM	10	Varied	Varied	Varied	Varied	NA	NM	1	NA	NM	NA	NM
3	2007	Mitrovic and Peterson [22]	E	Single	Heating	Water Marlotherm oil	NA	Resistance heater	SS	10	72	42	3.4	1000	300	0.8	3	10 *	T	NA	Vertical
4	2007	Mitrovic and Peterson [23]	E	Two	Heating	Water	Condensation	Isopropanol	SS	10	72	42	3.4	1000	300	0.8	3	10 *	T	Concurrent	Vertical
5	2007	Mitrovic and Peterson [24]	E	Single	Heating	Water Marlotherm oil	NA	Resistance heater	SS	10	72	42	3.4	1000	300	0.8	3	10 *	T	NA	Vertical
				Two	Condensation	Water	Condensation	Isopropanol	SS	10	72	42	3.4	1000	300	0.8	3	10 *	T	Concurrent	Vertical
6	2008	Maletic and Mitrovic [25]	N	Single	Heating	Water	NA	NA	NM	10	Varied	Varied	Varied	Varied	Varied	NM	1	NA	NM	NA	NM
7	2011	Mitrovic and Maletic [26]	N	Single	Heating	Pure water	NA	NA	NM	10	Varied	Varied	Varied	Varied	Varied	NM	1	NA	NM	NA	NM
8	2014	Piper et al. [5]	E / N	Single	Heating	Water	NA	NA	AISI304 AISI316L AISI321 AISI316Ti	10	21	72	3	NA	NA	NM	1	NA	L	NA	NM
9	2014	Tran et al. [27]	E	Two	Heating	Water	Condensation	Steam[%]	AISI321	10	42	72	3	1000	300	1	3	NM	L	NM	Vertical
					Heating	Water	Condensation	Chlorobenzene[%]	AISI321	NM	NM	NM	8	1800	500	1.5	6	12 #	NM	NM	Vertical
10	2014	Piper et al. [28]	N	NA	NA	NA	NA	NA	AISI304 AISI316L AISI321 AISI316Ti	8...20	NM	NM	1...12	NM	NM	0.5...2	NM	h_i...30	L M E	NA	NA
11	2014	Goedecke and Scholl [29]	E	Two	Condensation	Steam	Evaporation	Water Water+glycerol (71mol%)	NM	NM	NM	NM	NM	800	220	1.5	3	NM	NM	Counter current	Vertical
12	2015	Tran et al. [30]	E / N	Two	Heating	Water, monoethylene glycol (MEG) and water-MEG mixtures	Heating	Resistance heater	AISI321	10 10 12	72 42 42	42 72 72	3.4 3 7	1000 1000 1000	300 300 300	0.8 1 1	NM NM NM	NM NM NM	T L L	NA	Vertical
					Heating	Water	Condensation	Chlorobenzene[%]	AISI321	12	80	70	8	1800	500	1.5	6	12	T	NM	Vertical
13	2015	Goedecke and Scholl [31]	E	Two	Condensation	Steam	Evaporation	Water Water+glycerol (71mol%)	AISI316Ti	8	42	62	9	800	220	1.5	3	13	L	Counter current	Vertical
14	2015	Piper et al. [18]	N	NA	NA	NA	NA	NA	AISI304 AISI316L AISI321 AISI316Ti	10 10.5 10.5 10.5	55 42 42 42	95 42 62 72	9 Varied	NM	NM	NM	NA	NA	L E L L	NA	NM

(*continued on next page*)

Table 1 (*continued*)

												Varied							
												Varied							
15	2015	Piper et al. [32]	E	Single	NA	NA	Isothermal	Demineralized water	NM	10	55	95	8	1500	405	1.5	1	NA	L	NA	Vertical
16	2015	Siebeneck et al. [15]	E	Single	NA	NA	Isothermal	Deionized water	SS	NM	NM	NM	NM	NM	NM	NM	1	NA	NM	NA	Vertical
17	2015	Piper et al. [33]	E / N	Single	NA	NA	NM	Water	Steel	12	42	72	7	1000	270	NM	2	13	L	NA	NM
18	2015	Tran et al. [34]	E	Single	Heating	Water, monoethylene glycol (MEG) and water-MEG mixtures	Constant heat flux	Resistance heating	AISI321	10	72	42	3.4	1000	300	0.8	1	NA	T	NA	Vertical
										10	42	72	3	1000	300	1	1	NA	L		
										12	42	72	7	1000	300	1	1	NA	L		
19	2015	Goedecke and Scholl [35]	E	Two	Condensation	Steam	Evaporation	Water	AISI316Ti	8	42	62	9	800	220	1.5	3	13	L	Counter current	Vertical
20	2015	Rekstad et al. [36]	E / N	Two	Cooling/ heating	R744 (CO_2)	Evaporation/ condensation	RSW	SS	NM	NM	NM	NM	580	470	NM	3	NM	NM	NM	Vertical
														2000	500		6				
														2000	500		12				
21	2016	Piper et al. [20]	E / N	Single	Heating	Water	NA	NA	AISI321	10	72	42	3	NA	NA	NM	1	NA	T	NA	NM
										10	72	42	6						T		
										10	57	42	3						T		
										10	57	42	6						T		
										10	42	42	3						E		
										10	42	42	6						E		
										10	42	50	6						M		
										10	42	57	6						M		
										10	42	60	3						L		
										10	42	60	6						L		
										10	42	64	3						L		
										10	42	64	6						L		
										10	42	68	3						L		
										10	42	68	6						L		
										10	42	72	3						L		
22	2016	Piper et al. [37]	N	Single	NM	Water	NM	Water	NM	12	42	72	7	NA	NA	1	2	13	L	NA	NM
23	2016	Eldeeb et al. [2]	N	Single	NM	Water	NA	NA	AISI321	3...10	Varied	Varied	3...12	NA	NA	NM	1	NA	NM	NA	NM
24	2016	Rekstad and Ladam [38]	E	Two	Cooling/ heating	R744	Evaporation/ condensation	RSW	Steel	NM	NM	NM	NM	NM	NM	NM	12	NM	NM	NM	Vertical
25	2017	Arsenyeva et al. [16]	S	Single	Heating	Water	Cooling	Water	AISI321	NM	42	72	3.4	1000	300	0.8	NM	15.4 #	NM	NM	NM
										NM	72	42	3	1000	300	1	NM	15 #			
										NM	72	42	7	1000	300	1	NM	19 #			
26	2017	Piper et al. [9]	N	Single	Heating	Water	NA	NA	NM	7.2	72	42	6	NA	NA	NM	1	NA	T	NA	NM
										8.6	72	42	6						T		
										10	72	42	4.5						T		
										7.2	42	42	6						E		
										7.2	42	72	6						L		
										8.6	42	72	6						L		

(*continued on next page*)

Table 1 (*continued*)

										10	42	72	4.5						L			
27	2017	Tran et al. [39]	E	Two	Evaporation	R134a	Condensation (mimicked)	Resistance heating	AISI321	NM	NM	NM	7	1000	300	1	1	NA	NM	NA	Vertical
28	2017	Zhang et al. [40]	E / N	Single	Heating	Water	Cooling[$]	Water[$]	SS	12	60	NM	7.6	800	200	NM	NM	NM [$]	NM	Counter current[$]	NM
29	2018	Eldeeb et al. [1]	N	Single	Heating	Water	NA	NA	AISI321	3...10	Varied	Varied	3...12	72	NA	0.15	1	NA	NM	NA	NM
30	2018	Eldeeb et al. [41]	N	Single	Heating	Water	NA	NA	AISI321	Noncircular	Varied	Varied	3...12	NM	NA	NM	1	NA	NM	NA	NM
31	2018	Arsenyeva et al. [42]	E / N	Single	Heating[$]	Water	Cooling	Dry air	AISI304	6	36	42	3.5	530	230	0.8	2	15.5[#]	M	Counter current[$]	NM
32	2018	Arsenyeva et al. [43]	E	Single	Heating	Water	Cooling	Dry air	AISI304	6	36	42	3.5	530	230	0.8	2	15.5[#]	M	Counter current	NM
33	2018	Vocciante et al. [44]	N	Single	NA	NA	Isothermal	Water	NM	NM	NM	NM	NM	NM	NM	NM	2	NM	NM	NM	NM
34	2018	Tran et al. [6]	S	NA	NA	NA	NA	NA	NA	NA	NA	NA	NA	NA	NA	NA	NA	NA	NA	NA	NA
35	2018	Tran et al. [12]	S	NA	NA	NA	NA	NA	NA	NA	NA	NA	NA	NA	NA	NA	NA	NA	NA	NA	NA
36	2018	Scholl [45]	S	NA	NA	NA	NA	NA	NA	NA	NA	NA	NA	NA	NA	NA	NA	NA	NA	NA	NA
37	2018	Zibart and Kenig [46]	N	Multi	NA	NA	NA	Water+air	NM	10	55	95	9	1000	55	NM	1	NA	L	NA	Vertical
38	2018	Kumar et al. [47]	N	Single	Heating	Water	NA	NA	AISI304	10	72	42	3.4	367.5	36	1	1	NA	T	NA	Vertical
39	2019	Piper et al. [48]	N	Single	NA	NA	Cooling	NM	NM	10	42	72	6	NA	NA	1	2	9	L	NA	NM
40	2019	Goedecke and Scholl [49]	E / N	Two	Condensation	Steam	Evaporation	Water Water+glycerol (71mol%)	NM	NM	NM	NM	NM	NM	NM	1.5	>1	NM	NM	NM	Vertical
41	2019	Arsenyeva et al. [50]	S	Single Single	Heating Cooling	Water Products	Cooling Heating	Water Crude oil	AISI321	NM NM NM	72 42 42	42 72 72	3.4 3 7	1000 1000 1000	300 300 300	0.8 1 1	NM	NM	NM	Counter current	NM
42	2019	Arsenyeva et al. [19]	E / N	Single	Heating	Water	Cooling	Air	AISI304	6	36	42	3.5	530	230	0.8	2	15.5[#]	M	Counter current	NM
43	2019	Kumar et al. [51]	N	Single	Heating	Water	NA [$]	NA	NM	10	72	42	3	367.5	36	NM	1	NA	T	NA	Vertical
										10	72	52	3	367.5	36				T		
										10	72	62	3	367.5	36				T		
										10	72	72	3	367.5	36				E		
										10	42	42	3	367.5	21				E		
										10	52	42	3	367.5	26				T		
										10	62	42	3	367.5	31				T		
										10	72	42	3.4	367.5	36				T		
										10	72	42	4	367.5	36				T		
										10	72	42	5	367.5	36				T		
										10	72	42	6	367.5	36				T		
										6	72	42	3	367.5	36				T		
										8	72	42	3	367.5	36				T		
										12	72	42	3	367.5	36				T		
44	2019	Shirzad et al. [52]	N	Single	Heating	Al_2O_3-water CuO-water TiO_2-water	Constant heat flux	NA	NM	NM	NM	NM	NM	NM	NM	NM	1	NA	NM	NA	NM
45	2019	Shirzad et al. [53]	N	Single	Heating	Water	Constant heat flux	NA	NM	10	42	72	3	NM	42	1	1	NA	L	NA	NM
										10	42	72	4.5		42				L		
										10	42	72	6		42				L		
										10	42	72	7.5		42				L		
										10	42	53	4.5		42				M		
										10	42	61	4.5		42				L		
										10	42	72	4.5		42				L		
										10	42	88	4.5		42				L		
										10	51	50	4.5		51				T		
										10	60	50	4.5		60				T		
										10	74	50	4.5		74				T		
										10	95	50	4.5		95				T		
46	2019	Arsenyeva et al. [54]	E	Single	Heating	Water	Cooling	Dry air	AISI304	6	36	42	3.5	530	230	0.8	2	15.5[#]	M	NM	NM
47	2019	Selvnes et al. [17]	E	Two	Condensation/ evaporation	R744	Melting/ solidification	Water	NM	NM	30	50	NM	1500	750	NM	20	50	NM	NA	Horizontal
48	2019	Selvnes et al. [55]	N	Two	NA [$]	NA	Melting/ solidification	Water	NM	NM	30	50	NM	1500	750	NA	2	50	NM	NA	Horizontal
49	2019	Selvnes et al. [56]	N	Two	NA [$]	NA	Melting/ solidification	Water	NM	NM	30	50	6	1500	750	NA	2	56[#]	NM	NA	Horizontal
50	2019	Kumar et al. [57]	N	Single	Heating	Water	NA [$]	NA	NM	10	72	42	3.4	NA	NA	NM	1	NA	T	NA	Vertical
										10	42	72	3.4	NA	NA	NM	1	NA	L	NA	
51	2020	Eldeeb et al. [58]	N	Single	Heating	Water	NA	NA	AISI321	3...10	Varied	Varied	3...12	72	NM	0.15	1	NA	NM	NA	NM
				Single	Heating	Water	NA	NA	AISI321	Noncircular	Varied	Varied	3...12	NM	NM	NM	1	NA	NM	NA	NM
52	2020	Lin et al. [59]	E	Two	Cooling/ heating	Water	Melting/ solidification	Sodium acetate	SS	NM	NA	NA	NM	500	250	2	15	18	NA	NA	NM
53	2020	Selvnes et al. [60]	E	Two	Condensation/ evaporation	R744	Melting/ solidification	Water	SS	NM	NM	NM	NM	1480	740	NM	9	50	NM	NA	NM
54	2020	Sevault and Næss [61]	E	Two	Cooling/ heating	Water	Melting/ solidification	Commercial PCM	SS	NM	NM	NM	NM	NM	NM	NM	24	40	NM	NA	Vertical
55	2021	Selvnes et al. [62]	E	Two	Condensation/ evaporation	R744	Melting/ solidification	Commercial PCM	SS	NM	NM	NM	NM	1480	740	NM	10	15	NM	NA	Horizontal
56	2021	Selvnes et al. [63]	E	Two	Condensation/ evaporation	R744	Melting/ solidification	Water	SS	10	30	50	4.3	1480	740	1	10	15	L	NA	Horizontal
										10	30	50	4.3	1480	740	1	10	30	L		
										10	30	50	4.3	1480	740	1	10	45	L		
57	2021	Zibart and Kenig [4]	N	Single	Heating	Water	Cooling	Water	Aluminum	12	42	72	7	504	21	1	2	13	L	Counter current	NM
									SS	12	42	72	7	504	21	1	2	13	L		
									Aluminum	12	42	72	7	504	21	2	2	13	L		
									SS	12	42	72	7	504	21	2	2	13	L		
58	2021	Al-Turki et al. [64]	N	Two	Heating	Al_2O_3-water	Constant heat flux	NA	NA	10	42	72	6	72	42	NM	1	NA	L	NA	NM
										10	72	42	6	42	72	NM	1	NA	T		
59	2021	Guo et al. [65]	E	Single	Heating	Water	Condensation	Steam	AISI316L	NM	NM	NM	NM	NM	NM	NM	NM	NM	NM	Crossflow	Horizontal

[&]E:experimental/N:numerical/S:summary
[^]E:equidistant/L:longitudinal/M:mixed/T:transversal/NM:not mentioned/NA:not applicable
[+]The definition of outer channel distance was unclear
[%]With noncondensable (N_2)
[$]Not applicable in simulations (constant wall temperature)
[#]Calculated according to Figure 3

Table 2
Objectives of studies on PPHXs.

Objective	Number*
The geometry having best heat transfer	1 2
Correlation: friction factor (IC)	3 5 12 18
Correlation: Nusselt (IC)	3 6 12 18
Correlation: friction factor (OC)	4 5 17 30 31 36 40 42 46
Correlation: Nusselt (OC)	4 5 30 31 36 40 42
Investigation: pitch pattern	21
Investigation: fluid flow (IC/OC)	22 57
Investigation: turbulence	33 51
Investigation: thermohydraulic	38
Investigation: different PPHX scales	9 12
Investigation: weld pattern	6
Investigation: weld shape	8 21 29 59
Optimization: weld shape	52
Optimization: thermohydraulic#	22 29 30 52
Characterization: geometric parameters	10 15 23 26 34
Characterization: falling film over pillow-plates	16 17 37
Design approach development	24 41
Parametric study	43 44
Heat transfer enhancement: dimples	39
Heat transfer enhancement: nanofluids	45 59
Analysis: exergy and entransy	28
Analysis: crack failure	60
Comparison: smooth PHXs	28
Comparison: chevron PHXs	52
Application: condenser	9 12 18 20 28 35
Application: evaporator	20 28
Application: reboiler	11 14 19 40
Application: thermal storage	48 49 50 54 55 56 57 58

* Numbered according toTable 1.
\# Maximizing heat transfer coefficient and minimizing pressure drop.

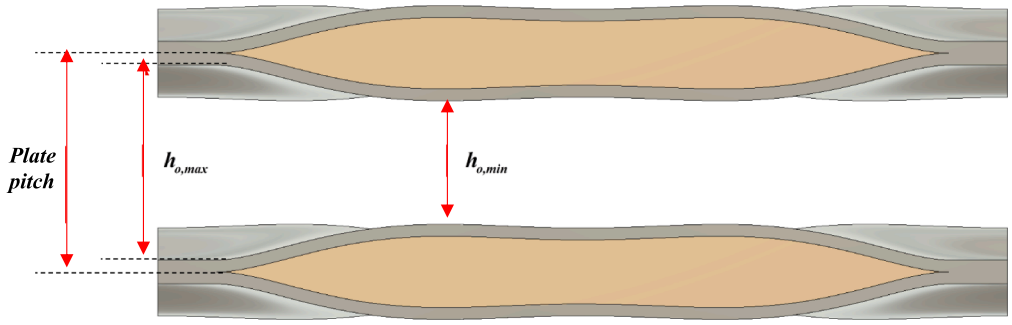

Fig. 3. Definition of outer channel maximum and minimum distance as well as plate pitch.

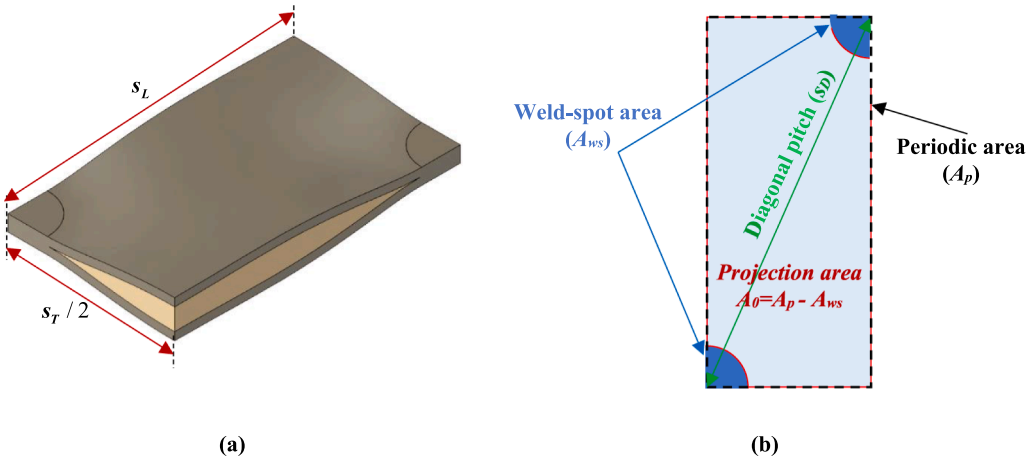

Fig. 4. Schematic representation of (a) a periodic section and (b) some geometrical parameters.

suitability for high pressure applications. Aside from high thermal conductivity, aluminum benefits from low density (lightweight PPHXs) and better flexibility (easier forming), as well as lower carbon footprint with production using renewable power. Aluminum plates have shown 10–25% lower thermal resistance compared to SS plates, bringing several benefits (hydrodynamic, thermal and economic) [4]. Titanium has also been recommended for refrigerated seawater (RSW) systems [8]. Overall, more research is needed to find suitable materials for different applications.

2.4. PPHX configurations

2.4.1. Embossing

Fig. 5 shows some possible embossing configurations. If the sheets are identically thick, the inflation would be homogeneous (double-embossed configuration); however, if one sheet is thicker than the other, only the thinner one would be inflated (single-embossed configuration) [6]. The latter is commonly used in jacketed vessels (e.g., dryers, reactors [4]). Note that designs with more than one IC (although not

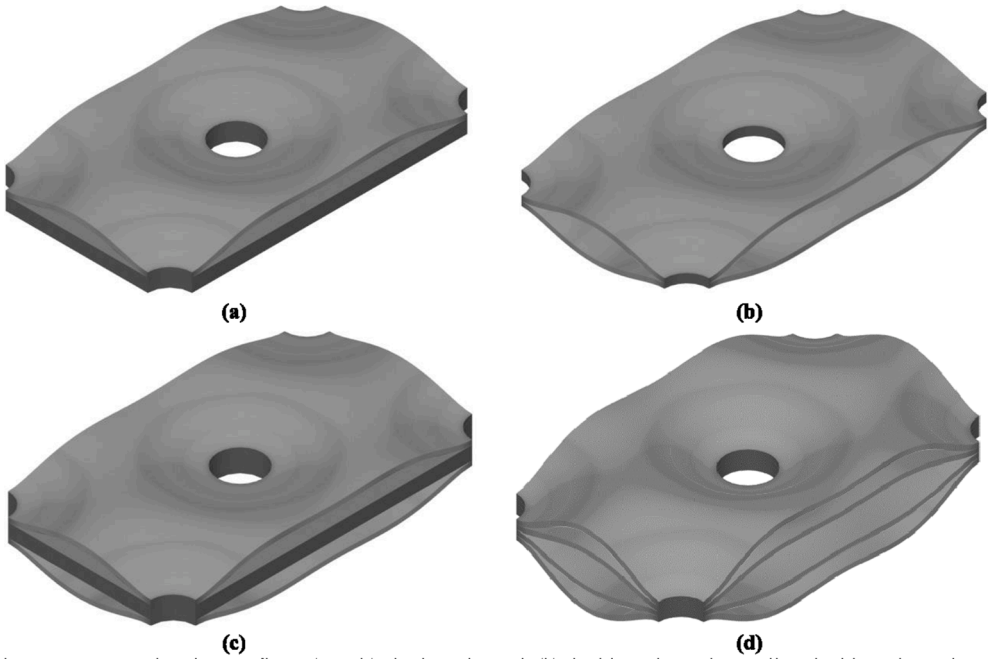

Fig. 5. PPHX embossing configurations. (a) single embossed, (b) double embossed as well as double embossed with (c) two and (d) three inner channels (). adapted from [6]

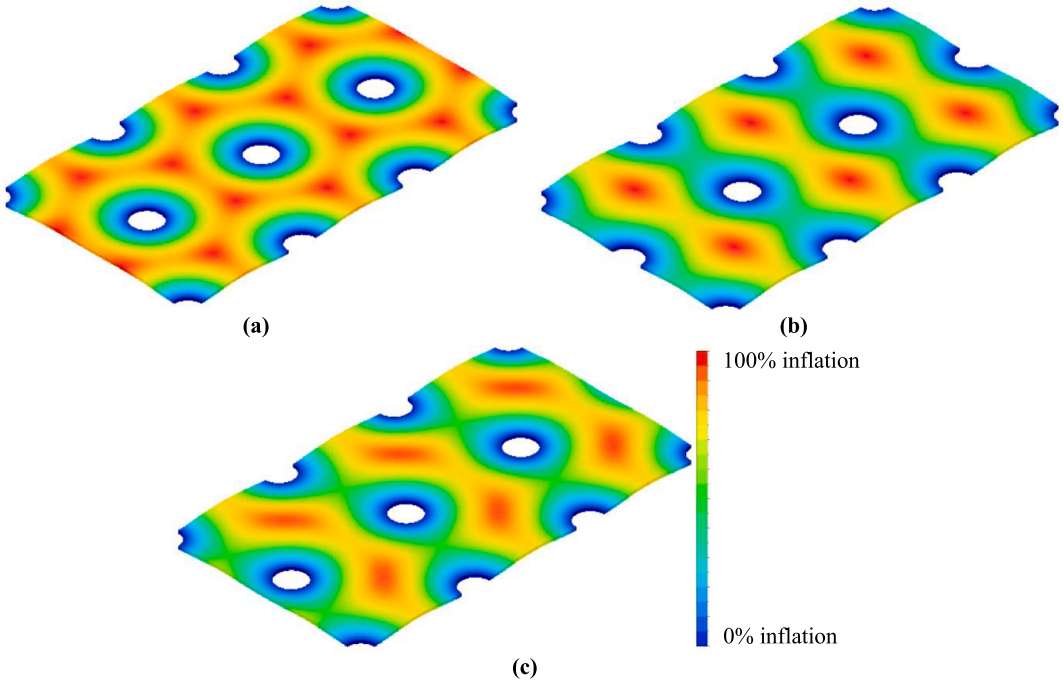

Fig. 6. PPHX weld-spot patterns. (a) triangular (or staggered), (b) rectangular (or parallel) and (c) hybrid.

common) are possible but have never been investigated.

2.4.2. *Weld-spot pattern*

Similar to tube patterns in STHXs, there are two common patterns for PPHXs known as triangular (or staggered) and rectangular (inline or parallel) patterns shown in Fig. 6a and b (indicating inflation contours). It is also possible to develop other arbitrary patterns or some patterns between these two (denoted by hybrid patterns) an example of which is shown in Fig. 6c. Generally, triangular patterns are the most common ones mainly due to their structural stability and thermohydraulic performance [20]. According to Table 2, Mitrovic and Maletic [25] conducted the only study investigating the effect of WS pattern where triangular, rectangular and hybrid WS patterns were compared in terms of their thermohydraulic performance. However, their results cannot be confidently adopted (their unvalidated model was based on laminar flow assumption) and further research is needed.

2.4.3. *Weld-spot shape*

Circular shapes are commonly used in PPHXs; however, other shapes are also possible. Elliptical shapes have also been investigated due to

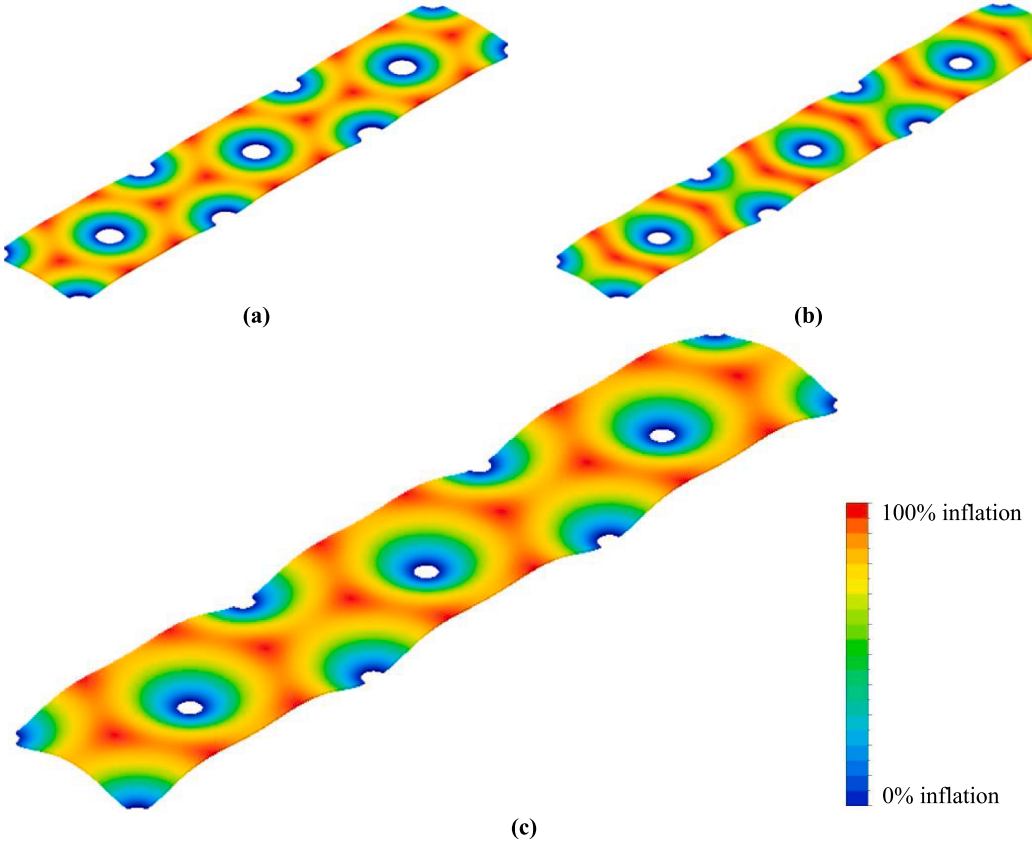

Fig. 7. PPHX longitudinal pitch patterns. (a) "conventional" [18], (b) "untypical surface waviness" [18] and (c) counterexample for "untypical surface waviness".

their more streamlined configuration. Besides, according to Table 2 some studies tried to optimize the WS shape to achieve the best thermohydraulic performance. More details about these studies are provided in Section 6.3.

2.4.4. Pitch pattern

The pitch pattern is commonly used to define transversal, longitudinal or equidistant configuration. However, there is a conflict between the study of Eldeeb et al. [1] and that of Piper et al. [20] in terms of defining transversal and longitudinal PPHX types. The former called a PPHX transversal/longitudinal for a pitch ratio (Equation (1)) lower/higher than 1; however, Piper et al. used the reduced WS pitch (Equation (8)). To make the content harmonized and due to the higher number of investigations conducted by Piper et al., their definition is utilized in this study.

Geometrically, in equidistant pitch pattern (where the longitudinal and transversal pitches are equal), s_R value is one, while values greater/smaller than one represent longitudinal/transversal pitch patterns:

$$\begin{cases} s_R > 1 & Longitudinal \\ s_R = 1 & Equidistant \\ s_R < 1 & Transversal \end{cases} \tag{9}$$

However, after a scrutinized numerical analysis of flow behavior, three types of PPHX were identified based on the s_R value [20]:

$$\begin{cases} s_R > 1.56 & Longitudinal \\ 1 < s_R \leqslant 1.56 & Mixed \\ s_R \leqslant 1 & Transversal \end{cases} \tag{10}$$

Nevertheless, in this study, the term "equidistant" was maintained for $s_R = 1$. According to Table 1, the study of Piper et al. [20] was the most comprehensive study in terms of considering different pitch patterns. Overall, most of the studies focused on longitudinal followed by transversal pitch pattern. Equidistant and mixed patterns were also investigated but much less than the rest.

It is worth mentioning that Piper et al. [18] denoted pillow-plates with longitudinal pitch pattern with s_{ratio} values below and above 1.75 as "conventional" (Fig. 7a) and "untypical surface waviness" (Fig. 7b), respectively. For the latter, the WSs in the transversal direction are located much closer than the longitudinal direction. Consequently, once hydroformed, the cross-sectional area is almost constant in the transversal direction (recognizable by the red sections in the transversal direction in Fig. 7b showing the maximum inflation). In contrast, "conventional" pillow-plates have almost hexagonal red contours around each WS. It is worth mentioning that the threshold s_{ratio} value of 1.75 seems to be limited to the cases studied by Piper et al. [18] (see Table 1) and a counterexample is shown in Fig. 7c with the same WS diameter (10/80/160/5:$d_{ws}/s_T/2s_L/h_i$). In this case, despite s_{ratio} value of 2, the surface waviness is not "untypical" (observable from the hexagonal red contours around each WS, similar to Fig. 7a). The readers are therefore cautioned to consult the geometric range covered by Piper et al. [18] when applying this criterion. Nevertheless, no further attempt was made since this is beyond the scope of this review study.

2.4.5. Flow configuration

PPHXs can handle single as well as two-phase flows and they are compatible with concurrent, crossflow and countercurrent flows [15]. Concurrent and counter current flows have already been studied in the literature; however, crossflow configuration has been investigated only once (see Table 1). Therefore, further studies are required to fill this gap in the literature.

2.4.6. Orientation

The PPHXs investigated so far were mostly vertically oriented;

Table 3
Chronological summary of experimental studies on PPHX indicating the measured parameters and experimental equipment.

		Number*																												
		3	4	5	8	9	11	12	13	15	16	17	18	19	20	21	27	28	31	32	40	42	47	52	53	55	56
Measured parameter	Temperature	•	•	•	•	•	•	•	•	•			•	•	•	•	•	•	•	•	•	•	•	•	•	•	•
	Flow rate				•	•		•	•					•	•	•	•	•					•	•			
	Mass flow rate		•	•			•		•		•	•	•	•	•		•			•	•	•			•		•
	Density				•	•		•						•		•			•	•		•					
	Voltage		•	•	•	•		•					•			•						•					
	Pressure					•	•	•	•			•	•	•	•	•	•		•	•			•	•	•	•	•
	Differential pressure		•	•	•	•		•	•			•	•		•	•	•	•	•	•			•	•	•	•	•
	Level[#]						•		•					•													
	Weight[&]						•		•					•													
Equipment	UV light									•	•																
	Camera									•	•																

* Numbered according to Table 1.
\# Used for hydrostatic pressure.
& To determine the amount of product condensate.

however, they can also be used horizontally or even inclined. Nevertheless, a comparison between the performance of PPHXs oriented horizontally, vertically and inclined is currently missing from the literature. Overall, since PPHXs can be oriented vertically or horizontally, they can be useful for applications with limited space [38].

3. Experimental protocol

According to Table 2, the most common objective for experimental studies were (1) correlation development for friction factor and Nusselt, (2) characterization of falling film over pillow-plates, (3) specific PPHX applications. Therefore, the experimental protocol varied based on the objective. Nevertheless, they share some characteristics (as shown in Table 3):

- **Temperature measurement:** Most studies conducted temperature measurement which was mostly used for Nusselt correlation development. The measurements were conducted primarily using thermocouples (e.g., B, K, or T-type) or RTDs (e.g., Pt100).
- **Flow measurement:** Almost all studies considered flow measurement, especially for flow regulation within and/or between pillow-plates. Note that mass and volume flow rate measurements are differentiated in Table 3.
- **Density measurement:** Few studies also measured the density which was primarily used to calculate the HTF mass flow rate.
- **Voltage measurement:** In some studies, a resistance heater was used for heating and voltage drop was measured to determine the energy delivered to the HTF.
- **Pressure measurement:** Evaluation of pressure and differential pressure was considered in several studies. Note that some studies used these terms interchangeably making difficulties for compiling Table 3. They were mostly used for correlation development for friction factor. It is worth pointing out that level sensors were also considered in some studies to measure the hydrostatic pressure.
- **Weight measurement:** Weight was measured in a series of studies [29,31,35] where it was used to determine the amount of product and steam condensates (i.e., application PPHX as reboiler).
- **Camera and UV light:** Such equipment was used to visualize falling film over pillow-plate surfaces. Digital high-speed and high-resolution cameras were used to capture wave dynamics over the surfaces.

At the time of writing this paper, to the best of the authors' knowledge, no standardized procedure exists for PPHX thermo and/or hydraulic performance testing. It is recommended that such procedures are developed to harmonize the studies and minimize experiment-specific errors and/or bias. Given the wide variety of PPHX design parameters, such procedures would be required to compile a coherent database for their performance.

4. Numerical advancements

A motivation for numerical investigations of PPHXs is that they have several design variables. Thus, there are too many possible design combinations, making experiments complicated and expensive. In this section, some details for numerical analysis of PPHXs are discussed.

4.1. Formation

4.1.1. Mathematical functions

In earlier numerical studies, mathematical expressions (e.g., trigonometric functions) were used to generate pillow-plate geometries (see Table 4). This results in the maximum inflation height at the intersection of each four surrounding WSs. However, in reality, the highest inflation (of pillow-plates with non-equidistant pitch pattern) is formed with an offset from the intersection, closer to the WSs having the higher pitch

Table 4
Mathematical functions developed to mimic the PPHX formation process.

Ref.	Mathematical function*	Application$	Comment
[7,21,25,26]	$y = \pm\frac{\delta}{4}\left[1+\cos\left(\frac{2\pi}{s_T}z\right)\cos\left(\frac{\pi}{s_L}x\right)\right]$	Triangular WS pattern	
[25]	$y = \pm\frac{\delta}{8}\left[2-\cos\left(\frac{\pi}{s_L}(x-c)\right)\cos\left(\frac{4\pi}{s_T}z\right)\right]$	Rectangular WS pattern	*c*:a positive constant Typo in the reference
[25]	$y = \pm\frac{\delta}{2}\left[1-\sum_{i=1}^{N}\exp\left\{-c\left[(x-x_{0i})^2+(z-z_{0i})^2\right]\right\}\right]$	All	*c*:a positive constant

* The functions were updated according to Fig. 2b.
$ SeeFig. 6.

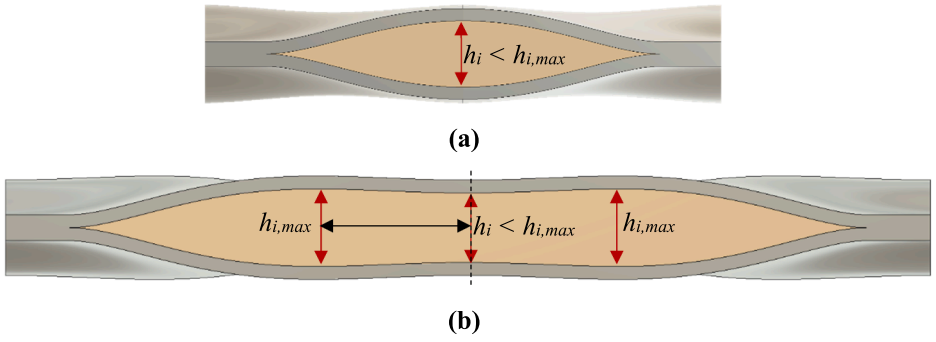

Fig. 8. Maximum inflation height for cross-sectional view in the direction of (a) smaller pitch and (b) higher pitch.

value (see Fig. 8) [6]. For longitudinal pitch pattern, the offset was found to be $s_L/3$ [18]. Therefore, the main limitation for using mathematical functions for geometry reconstruction is that it is not representative of the actual surface characteristics [7,25,26].

4.1.2. Structural formation

In this type, the hydroforming process is numerically reconstructed using a commercial software (e.g., Abaqus [66]). Encastre (i.e., zero degree of freedom) condition is applied at the WSs, whereas a hydrostatic pressure is exerted over the plates to achieve expansion [51]. This pressure load should be imposed evenly/gradually to prevent local deformation and achieve quasi-steady-state conditions (preventing viscoplastic effects) [5]. Symmetrical boundary conditions are commonly used to simplify the geometry. Benefits of structural reproduction include [5]: (1) mimicking the hydroforming process (less than 4% error), (2) possibility to apply for any arbitrary WS pattern, (3) obtaining the local stress values which can be used for deformation optimization.

4.2. Thermohydraulic analysis procedure

A powerful method of conducting numerical analysis on thermohydraulic behavior of pillow-plates is using computational fluid dynamics (CFD). According to Table 5, several numerical studies using CFD were conducted on PPHXs in the past. Briefly, earlier studies used mathematical formation and were focused on laminar flow. But current state-of-the-art uses structural formation and adopts a turbulence model (see Section 4.3).

A major shortcoming of some studies is the lack of model validation. For earlier studies this was due to the lack of (or hard accessibility to) experimental data. However, several experimental studies have since been conducted (presented in Section 3), making data abundantly available to researchers. Future numerical studies are urged to make use of such data for model validation.

Another interesting shortcoming is the low number of optimization studies. As explained in Section 2, PPHXs have multiple design parameters, configuration, etc. Therefore, optimization studies would be needed to find the most capable geometry/configuration. Otherwise, the literature would be stranded (as it has been so far to some extent) to figure out the most efficient designs. Note that some studies mentioned optimization interchangeably for parametric studies.

4.3. Common assumptions and boundary conditions

The most common assumptions for CFD simulation of PPHXs include (see Table 6):

- 3D turbulent, incompressible, steady-state fluid flow
- Constant fluid thermophysical properties
- No-slip condition at walls
- Constant inlet temperature
- Constant wall temperature or constant wall heat flux

Note that WSs and the subsequent flow deflection cause turbulence at lower Reynolds in PPHXs compared to typical pipe flow. Therefore, turbulence modeling should be considered; otherwise, the laminar flow assumption underestimates the pressure drop at higher Reynolds [3].

Aside from direct numerical simulation (DNS), which is computationally demanding, the two main turbulence model categories include scale resolving simulation of large eddy simulation (LES) and Reynolds average Navier Stokes (RANS) [44]. Moreover, recently some hybrid models have been developed such as detached eddy simulation (DES). In PPHXs, standard k-ε turbulence model (a typical RANS model) was found to overestimate the IC heat transfer coefficient [9,20]. Most studies used realizable k-ε model (see Table 5) for which it has been recommended to use a two-layer model to capture the near-wall dampening of turbulence [4]. As such, Wolfshtein's model [67] is reduced for the region impacted by viscosity in which only k is solved while ε is algebraically determined, achieving better numerical stability. For OC, most studies used standard elliptic blending k-ε model (see Table 6); however, lag elliptic blending k-ε model was found to be more numerically stable with guaranteed steady-state solution [4]. A numerical study [44] was specifically conducted to evaluate several turbulence models for OC flow, based on RANS (realizable k-ε [68], RNG k-ε [69], SA [70], LL k-ε [71], k-kL-ω [72] and k-ω SST [73]), DES (DES k-

Table 5
Chronological summary of numerical studies on PPHX.

No.*	Study#	Channel	CFD software/algorithm				Formation method/software		Validation	Investigated parameter(s) and range
			StarCD	STAR-CCM+	ANSYS Fluent	OpenFOAM	Mathematical	Structural		
1	F/H	IC	SIMPLE				•		None	• s_L (reported s_{ratio}:0.35…infinity) d_{ws} (reported s_{dia}:~0.015…~0.06) Re (indirectly related):50…3800 L (not reported):maximum of 500 mm
2	F/H	IC	•				•		None	• s_L (reported s_L/L:0.025…infinity) s_T (reported s_T/L:0.08…0.2) h_i (reported hydraulic diameter:~2.4…~8.4 mm) Re (indirectly related):50…4000 L (not reported):maximum of 500 mm
6	F/H	IC	•				•		None	• s_L (not reported) s_T (not reported) h_i (not reported) Re (indirectly related):50…2000 L (not reported):maximum of 500 mm WS pattern: triangular/rectangular
7	F/H	IC	SIMPLE				•		None	• s_L:14…31.5 mm (also reported s_L/L:0.025…infinity) s_T:40…100 mm (also reported s_T/L:0.08…0.2) h_i (maximum of 3.4 mm, reported hydraulic diameter:2.5…8.4 mm) Re (indirectly related to others):50…4000 L (not reported):maximum of 500 mm
8	F/H	IC		•				Abaqus	Self	• Re:1080…8680WS shape: circular/elliptical (with the same transversal diameter but 1.5 times longitudinal diameter as circular)
10	S	NA						Abaqus	Self	• d_{ws}:8…20 mm h_i:1…12 mm δ:0.5…2mm B:h_i…30 mm s_R:1…2.08
12	F/H	IC		•					[5]	• HTF mass flux:~100…~1600 kg/m^{2}s
14	S	NA						Abaqus	[5]	• Hydroforming pressure Pitch ratio
17	F/H	OC		•				Abaqus	Self	• Re:9500…30000 Pr:6…150 Longitudinal plate offset:0…s_L Transversal plate offset:0…s_T/2
21	F/H	IC		•				Abaqus	[30,34]	• 2s_L:42/50/57/60/64/68/72 mm s_T:42/57/72 mm h_i:3/6mm Re (indirectly related):1000…8000 Weld shape: circular/elliptical
22	F/H	IC/OC		•				Abaqus	[30,33]	• Re_{OC}:5000…15000
23	F/H	IC			•			ANSYS Static Structural	None	• d_{ws}:3…10 mm h_i:3…12 mm s_{ratio}:0.4…1
26	F/H	IC		•				Abaqus	[30,34]	• Re:1000…8000 Pr:1…150 s_R:0.58/1/1.71 s_{dia}:0.1…0.24 (see Eq. (2)) s_{inf}:0.042…0.083 (see Eq. (3))

(*continued on next page*)

Table 5 (*continued*)

No.*	Study#	Channel	CFD software/algorithm				Formation method/software		Validation	Investigated parameter(s) and range
			StarCD	STAR-CCM+	ANSYS Fluent	OpenFOAM	Mathematical	Structural		
28	F/H	IC			SIMPLE				Self	• Cold HTF flow rate:200/400/600/800/1000L/h Hot HTF flow rate:500/1000/1500L/h
29	F/H	IC			SIMPLEC			ANSYS Static Structural	None	• d_{ws}:3…10 mm h_i:3…12 mm s_{ratio}:0.58…1.73 Inlet velocity:0.1…2m/s
30	F/H	IC			SIMPLEC			ANSYS Static Structural	None	• h_i:3…12 mm s_{ratio}:0.58…1.73 Inlet velocity:0.1…2m/s Weld height:3…10 mm (see Fig. 13b)WHR:1…2 (see Fig. 13b)
31	F/H	OC		•					Self	• *Re*:3000…20000
33	F	OC				PISO		Abaqus	[37]	• *Re*:3000…8000Turbulence models based on RANS (realizable k-ϵ/RNG k-ϵ/SA/LL k-ϵ/k-kL-ω/k-ω SST), DES (DES k-ω SST) and LES (SM/WALE)
37	F	OC		•				Abaqus	[32]	None
38	F/H	IC			•			Abaqus	[34]	• *Re*:1200/2800/4200/6500/7800
39	F/H	OC		•					[30,33]	• Surface: smooth/dimpled
40	F/H	OC							Self	• Operating pressure:0.1…1.0 bar Submergence:40…130% Overall temperature difference:5…20 °C
42	F/H	OC		•					Self	• Cold HTF flow rate:130…900 kg/h (*Re*:30…3500) Hot HTF flow rate:40…105 kg/h (*Re*:7500…16000) Hot HTF temperature:100…325 °C
43	F/H	IC			SIMPLE			Abaqus	[30,34]	• d_{ws}:6/8/10/12 mm $2s_L$:42/52/62/72 mm s_T:42/52/62/72 mm h_i:3/3.4/4/5/6mm *Re*:1200…7800
44	F/H	IC			SIMPLE				[30]	• *Re*:1000/2000/4000/6000/8000 Nanofluid:Al_2O_3/CuO/TiO_2 Volumetric nanoparticle concentration:0/2/3/4/5%
45	F/H	IC			SIMPLE				[30]	• h_i:3/4.5/6/7.5 mm $2s_L$:50/53/61/72/88 mm s_T:42/51/60/74/95 mm *Re*:1000/2000/4000/6000/8000
48	F/H	OC			SIMPLE				None	• Solidification mushy zone parameter:10^7/10^8/10^9 Melting mushy zone parameter:10^5/10^6/10^7/10^8 Phase change temperature range:0.5/1°C
49	F/H	OC			SIMPLE			Autodesk Inventor	None	None
50	F/H	IC				PIMPLE		Abaqus	[34]	• $2s_L$:42/72 mm s_T:42/72 mm
51	F/H	IC			•			ANSYS Static Structural	None	• d_{ws}:3…10 mm h_i:3…12 mm s_{ratio}:0.58…1.73 Inlet velocity:0.1…2m/s Weld height:3…10 mm (see Fig. 13b)WHR:1…2 (see Fig. 13b)
57	F/H	IC/OC		•				Abaqus and Autodesk Inventor	[9,33,37]	• Re_{IC}:1000/2000/3000 Re_{OC}:5000/7500/10000

(*continued on next page*)

Table 5 (*continued*)

No.*	Study#	Channel	CFD software/algorithm				Formation method/software		Validation	Investigated parameter(s) and range
			StarCD	STAR-CCM+	ANSYS Fluent	OpenFOAM	Mathematical	Structural		
58	F/H	IC							None	δ:1/2mm Plate material: pure aluminum/stainless steel • *Re*:250/500/750/1000 Volumetric nanoparticle concentration:0/1/2/3% Pitch pattern: longitudinal/transversalWeld shape: circular/elliptical (both inline and perpendicular to flow)

* Numbered according to Table 1.

\# F:fluid dynamics/H:heat transfer/S:structural formation.

ω SST [74]) and LES (SM [75] and wall adapting local eddy-viscosity denoted by WALE [76]). Compared with the experimental data, the best turbulence model to predict pressure loss and Darcy friction factor was DES *k*-ω SST model. In contrast, *k*-ω SST model had the worst performance with deviations exceeding 50%. Besides, the simple SA model [70] underestimated pressure loss by only 10% and can be suitable for general purpose CFD simulations.

The following sections discuss the common boundary conditions used for fluid flow and heat transfer. Note that symmetricity was commonly exploited to save computational power.

4.3.1. Inlet/outlet

Constant velocity, mass flow rate or pressure has been used at the inlet. Moreover, some studies used periodic boundary conditions at inlet and outlet (i.e., repeated velocity and turbulence fields) to achieve hydrodynamically fully-developed flow [5]. Consequently, the developing region was neglected as it represents a small PPHX portion at industrial scale [37]. This makes the simulation domain small (saving computational power); but the temperature field should be scaled to achieve a constant heat transfer coefficient (i.e., thermally fully-developed flow) [4].

4.3.2. Wall

Clearly, no-slip boundary condition should be used for CFD simulation of fluid flow at walls. Regarding heat transfer, according to Table 6, constant wall temperature (i.e., Dirichlet condition) has been used in multiple studies on the pillow-plate surface. A reason is to represent the two-phase heat transfer in the other channel. However, this boundary condition causes overestimation of heat transfer in OC (it is equivalent to a fin efficiency of one over the WSs [4]) and is not truly representative of experiments with resistance heating. In such cases, constant wall heat flux (i.e., Neumann condition) should be used. For the cases where both channels are to be simulated, conjugate heat transfer (CHT) should be applied. Alternatively, a simplified method exists to use the existing constant-wall temperature heat transfer coefficients together with some correction factors (see Section 5.4.2).

5. Thermohydraulic performance

5.1. Required geometric parameters

To evaluate thermohydraulic performance of PPHXs, heat transfer area, cross-section area, wetted area, volume and hydraulic diameter should be determined for the channel(s). Different definitions have been used especially in earlier studies; nevertheless, the recent literature used the definition/correlations developed by Piper et al. [18], summarized in Table 7. Normally, hydraulic diameter depends on the cross-sectional area and wetted perimeter. In PPHXs, these parameters change along the HTF direction; therefore, hydraulic diameter changes locally. However, determination of hydraulic diameter as shown in Table 7 (using its volumetric mean) is independent from the flow direction. In other words, whether the flow direction is longitudinal or transversal, as long as the same pitches are used, the hydraulic diameter would be the same [28]. Note that Table 7 is based on a single periodic section (see Fig. 4).

5.2. Performance parameters

According to Table 2, correlation development for friction factor and Nusselt number has been widely investigated. Some parameters have also been introduced to evaluate the thermohydraulic performance.

Friction factor is defined as:

$$\zeta = \frac{2d_h \Delta P}{\rho u_m L} \tag{11}$$

for which a power-law correlation known as “Blasius friction factor

Table 6
Summary of common assumptions in literature.

Objective	Assumption	1	2	6	7	8	10	12	14	17	21	22	23	26	28	29	30	31	33	37	38	39	40	42	43	44	45	48	49	50	51	57[$1]	57[$2]	58
CFD simulation	3D, incompressible, steady-state fluid flow	•	•	•	•	•		•		•	•	•	•	•	•	•	•	•	•		•	•		•	•	•	•			•	•	•	•	•
	Laminar flow	•	•	•	•																													•
	Turbulent flow[÷]					1		1		1	1	*IC* : 1 *OC* : 10	1	1	2	•	•	10	1...9		1	1	10		10	1	1	1			9	1	*IC* : 1 *OC* : 11	*IC* : 1 *OC* : 11	
	Constant fluid thermophysical properties	•	•	•	•	•		•		•	•	•						•				•		•	•		•					•	•	
	Temperature-dependent fluid thermophysical properties													•[*]												•								•
	No-slip condition at walls					•				•	•	•	•	•	•	•	•	•			•	•		•	•	•	•	•	•	•	•	•	•	•
	Constant inlet temperature (°C)	20	20	20	20	25		20		25			•		20	22	22	325			25	25	•	•	25	•	25	•[&]	•[&]		22	25	25	25
	Constant wall temperature (°C)	60	60	60	60	40				40	•	•	•	•	65	27	27	20			50				50					50	27	30	50	
	Constant wall heat flux (kW/m^2)																					0.5				•	5							5
	Homogeneous inlet velocity profile															•	•														•			
	Periodic flow boundary at inlet and outlet					•				•	•	•		•				•	•[@]			•								•		•		
	Thermally developed flow[#]					•				•	•			•	•																	•		
	Constant inlet mass flow rate																				•	•												
	Constant outlet atmospheric pressure[^]															•	•														•		•	
	Symmetricity at sides															•	•														•		•	
	WS temperature is equal to the rest of the pillow-plate																	•							•									
	Negligible radiation, natural convection and heat loss														•																			
	Negligible fouling resistance							•										•																
	Negligible gravity														•																			
	VOF method to capture the two-phase flow																			•														
	Continuum surface force (CSF) to consider surface tension																			•														
Reboiler modeling	Negligible subcooling																						•											
	Convective and nucleate boiling in the evaporation zone																						•											
Formation	Quasi-steady state[~]						•		•																									
	Elastoplastic and isotropic material behavior						•		•																									
	Clamped support[%] condition at WSs						•		•																									
	Continuum approach						•																											
	Thick shell approach[+]								•																									

[$1] Uncoupled simulations.
[$2] CHT simulations.
[÷] 1:realizable k-ε/2:RNG k-ε/3:SA/4:LL k-ε/5:k-k_L-ω/6:k-ω SST/7:DES k-ω SST/8:SM/9:WALE/10:elliptic blending k-ε/11:lag elliptic blending k-ε.
[*] Thermal conductivity, dynamic viscosity and specific heat capacity were polynomial functions of temperature (obtained from REFPROP).
[&] +/-5°C for melting/solidification.
[@] Decomposed the local pressure into linear and residual components.
[#] Constant heat transfer coefficient in the flow direction.
[^] 0Pa gauge.
[~] Gradual and even load.
[%] Zero degree of freedom.
[+] Negligible normal-to-wall stresses compared to tangential.

Table 7
Geometric parameters for thermohydraulic performance evaluation [18].

Property	Inner channel	Outer channel	Comment
Hydraulic diameter	$\overline{d}_{h,IC} = \frac{4V_{IC}}{A_{Wet,IC}}$	$\overline{d}_{h,OC} = \frac{4V_{OC}}{A_{Wet,OC}}$	Pillow-plate waviness causes cross-sectional area and wetted perimeter to change in the longitudinal direction. Thus, the average hydraulic diameter is commonly used.
Volume	$V_{IC} = f_V h_i s_D^2 f_{ws}$ $f_V = 0.1\left(\frac{s_T}{2s_L}\right)^2 - 0.18\left(\frac{s_T}{2s_L}\right) + 0.19$ $f_{ws} = 1.37\phi_A^{2.58}$	$V_{OC} = V_{Tot} - V_{IC} - V_P = \frac{s_L s_T}{2}\left(\frac{h_o}{2} + \delta_P\right) - V_{IC} - A_{wet,OC}\delta_P$	For ϕ_A see Eq. (4)
Wetted surface area	$A_{Wet,IC} = A_0\left(1 + f_A\frac{h_i^2}{s_D^2}\right)$ $f_A = 3.12\left(\frac{s_T}{2s_L}\right)^2 - 5.74\left(\frac{s_T}{2s_L}\right) + 3.08$	$A_{Wet,OC} = A_{Wet,IC} + A_{ws}$	For A_0 see Fig. 4
Cross-sectional area	$\overline{A}_{CS,IC} = \frac{V_{IC}}{s_L}$ $\overline{A}_{CS,IC,Tot} = \overline{A}_{CS,IC}4\left(\frac{W-2W_E}{s_T}\right)$	$\overline{A}_{CS,OC} = \frac{V_{OC}}{s_L}$ $\overline{A}_{CS,OC,Tot} = \overline{A}_{CS,OC}4\left(\frac{W-2W_E}{s_T}\right) + 2L_E(h_i + 2\delta_P)$	
Heat transfer area	$A_{HT,IC} = A_{Wet,IC}$ $A_{HT,IC,Tot} = A_{HT,IC}4\left(\frac{W-2W_E}{s_T}\right)\left(\frac{L-2L_E}{s_L}\right)$	$A_{HT,OC} = A_{Wet,OC}$ $A_{HT,OC,Tot} = A_{HT,OC}4\left(\frac{W-2W_E}{s_T}\right)\left(\frac{L-2L_E}{s_L}\right)$	The OC correlation excludes the edge surface area due to its negligible heat transfer

correlation" is common [20]:

$$\zeta = cRe^m \tag{12}$$

For two-phase flow an equivalent mass flow rate was used [24]:

$$\dot{m}_{eq} = \dot{m}\left[(1-q) + q\left(\frac{\rho_{liq}}{\rho_{vap}}\right)^{0.5}\right] \tag{13}$$

Note that in falling film studies, film Reynolds number is defined as [15]:

$$Re_f = \frac{\Gamma}{\mu} \tag{14}$$

Regarding the thermal aspect, as proposed by Dittus and Boelter [77], power-law correlations are commonly developed for Nusselt [12]:

$$Nu = cRe^m Pr^n \tag{15}$$

Other common formats using analogy between heat and mass transfer are those of Petukhov [78]:

$$Nu = \frac{\left(\frac{\zeta}{8}\right)RePr}{1.07 + 12.7\sqrt{\left(\frac{\zeta}{8}\right)}\left(Pr^{\frac{2}{3}} - 1\right)} \tag{16}$$

and generalized Lévêque equation (GLE) [79]:

$$\frac{Nu}{Pr^{\frac{1}{3}}} = \frac{Sh}{Sc^{\frac{1}{3}}} = 0.404\left(\frac{\zeta Re^2 d_h}{L}\right)^{\frac{1}{3}} \tag{17}$$

Besides, some earlier studies (on condensation) included Kapitza number and boiling number in their Nusselt correlations, which are defined as [24]:

$$Ka = \left(\frac{\rho_{liq}\sigma_{liq}^3}{g\mu_{liq}^4}\right)^{\frac{1}{3}} \tag{18}$$

$$Bo = \frac{\dot{q}A_{CS}}{\dot{m}\Delta H} \tag{19}$$

Thermohydraulic efficiency is defined as the transferred heat over the pumping power [20,37]:

$$\varepsilon = \frac{hA_W\Delta T}{\dot{V}\Delta P} \tag{20}$$

The ratio of thermohydraulic efficiency of a PPHX over a tube bundle having equal hydraulic diameters and temperature difference, has been considered as a performance parameter [37]:

$$\chi = \frac{\varepsilon_{PPHX}}{\varepsilon_{bundle}} = \frac{\left(\frac{hA_W}{\dot{V}\Delta P}\right)_{PPHX}}{\left(\frac{hA_W}{\dot{V}\Delta P}\right)_{bundle}} \tag{21}$$

Finally, performance evaluation criterion (PEC) is defined as [80]:

$$PEC = \left(\frac{h}{h_0}\right)\left(\frac{f_0}{f}\right)^{\frac{1}{3}} \tag{22}$$

where subscript 0 indicates the reference case.

5.3. Analysis of thermohydraulic behavior

5.3.1. Inner channel

Within IC, two types of flow can be identified [7]: (1) recirculation zones, established after WSs and (2) meandering core (MC) being constrained by the recirculation zones. Accordingly, as shown in Fig. 9, Piper et al. [9] developed the two-zone model where (as its name implies) two separate zones are considered for the recirculation zone and MC. The boundary layer in MC is fully-developed both thermally and hydrodynamically, while the flow within the recirculation zone is slow, resulting in a high gradient of wall shear stress [9].

However, the shape of the zones varies for different pitch patterns. In longitudinal and transversal pillow-plates, the recirculation zones formed behind the WSs have a "flame-like" shape (see Fig. 9) and straight shape (extended to the next WS), respectively [4]. In mixed pillow-plates, at lower Reynolds (i.e., below 2000) the flow is similar to longitudinal pillow-plates but at higher Reynolds values it transforms to the behavior observed in transversal pillow-plates.

For longitudinal pillow-plates, half of the total pressure loss is from form drag which weakly changes with Reynolds [9,20]. The reason is that form drag increases when recirculation zones are created (after WSs) whose size weakly varies with Reynolds in longitudinal pillow-plates. In contrast, in transversal pillow-plates, a smaller portion of the total pressure loss is from form drag with values decreasing by growing Reynolds. In mixed pillow-plates, form drag coefficient first increases with Reynolds (like transversal pillow-plates) followed by a weak change (like longitudinal pillow-plates). In contrast, regardless of

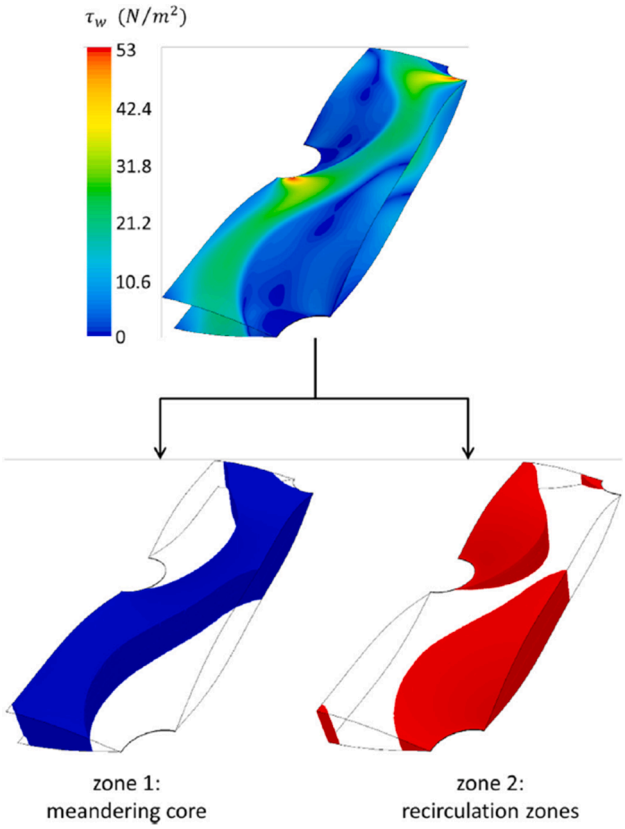

Fig. 9. Wall shear stress contour in IC and the concept of two-zone model by Piper et al. [9] (reprinted from International Journal of Thermal Sciences, 120, M. Piper, A. Zibart, E.Y. Kenig, New design equations for turbulent forced convection heat transfer and pressure loss in pillow-plate channels, 459–468, Copyright (2017), with permission from Elsevier).

the pillow-plate type, the friction drag coefficient behaves asymptotically when Reynolds increases. Consequently, the dimensionless Darcy friction factor behaves asymptotically (see Equation (12)).

The thermal behavior in pillow-plates is dictated by their hydraulic behavior where MC dominates the heat transfer, while recirculation zones have poor heat transfer, generating hotspots [20]. Moreover, WS-induced flow deflection enhances the heat transfer by lateral mixing [5].

For all pitch patterns, the highest thermohydraulic efficiency (see Equation (20)) is achieved at lower Reynolds [20]. This is due to the rapid pressure drop increase compared to heat transfer enhancement when increasing Reynolds. Besides, equidistant pitch pattern showed the lowest efficiency, while transversal pattern with the highest h_i showed the highest efficiency [20].

5.3.2. Outer channel

Unlike IC, the flow in OC has not yet been systematically characterized and the impact of pitch pattern is unclear. Overall, the plate waviness causes periodic acceleration/deceleration, resulting in boundary layer separation almost at the narrowest section of OC, upstream of WSs [48]. For longitudinal PPHXs, the vortex shape has been described as "tornado-like" (see Fig. 10) where the vortices spiral diagonally to the downstream WSs [37].

Using CHT, the highest heat flux was found to occur where the flow reattached after WSs due to the boundary layer thinning [4]. Moreover, the recirculation zone in IC was found to impact the OC heat transfer when the plate was made of SS (because of higher thermal resistance).

Regarding plate alignment, it can be offset in transversal/longitudinal direction. It was found that compared to no offset, displacing the neighboring plate by $0.5s_T$ improved PEC (see Equation (22)) by about

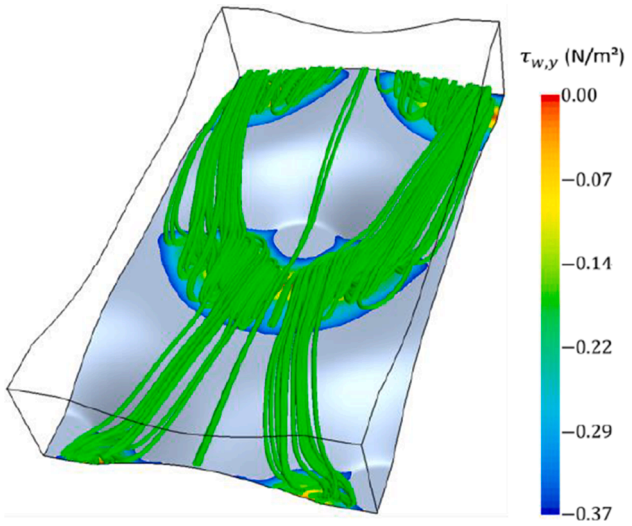

Fig. 10. Wall shear stress contour in OC indicating the streamlines [37] (reprinted from ASME Heat Transfer Summer Conference, 50329, M. Piper, J. Tran, E.Y. Kenig, A CFD study of the thermo-hydraulic characteristics of pillow-plate heat exchangers, Copyright (2016), with permission from ASME).

8% [33]. Therefore, optimization is needed to comprehensively analyze the impact of all design parameters and the offset.

5.3.3. General remarks

It has been repeatedly reported that the PPHX thermohydraulic performance depends on its configuration (outlined in Section 2.4). Despite that, several studies conducted mixed investigations (see Table 1), for instance by investigating both transversal and longitudinal configurations in the same study. The problem arises when they tried to draw universal conclusions, ignoring that these PPHXs are inherently different.

- **Longitudinal:** This pattern has received the greatest research attention and has shown superior heat transfer performance. Its OC flow has also been extensively investigated.
- **Transversal:** Although this pattern does not have the best heat transfer performance, but when also considering the pressure drop, it can outperform longitudinal pattern. However, its OC flow has not yet been properly characterized.
- **Mixed:** As its name implies, IC flow in mixed pattern behaves similar to the previous two depending on Reynolds. This has caused issues regarding its friction coefficient which has been commonly excluded from earlier studies. Overall, its OC behavior is not well-known.
- **Equidistant:** According to Table 1, equidistant pattern has not been extensively investigated. As they have the lowest thermohydraulic efficiency [20], further investigation seems unnecessary unless the OC flow (not investigated so far) brings considerable advantages.

5.4. Available correlations

5.4.1. Friction factor

Table 8 summarizes existing friction factor correlations for IC and OC, where most correlations are in Blasius format (see Equation (12)), making them specific to the unique geometry they were developed for (details in Table 1). In contrast, the two-zone model correlations (presented by IC9-11 in Table 8) have a wide application range but note that they have to be used together with their Nusselt correlations (presented in Section 5.4.2). The reason is that IC9-11 only represent the pressure losses caused by the wall shear stress in MC, excluding form drag; thus, they cannot reflect the total pressure drop.

In Table 8, more options are available for IC than OC. Moreover,

Table 8
Chronological summary of the correlations developed for friction factor.

Channel	HTF	Development	Format	Application[&]	Pattern	Correlation(s)	Deviation	Reference
Inner	●Water ●Marlotherm oil (single-phase)	Experimental	Blasius	Laminar: $1000 < Re < 2400$ Turbulent: $2400 < Re < 7500$	Transversal Transversal	(IC1)$\zeta = 1.1 \times 10^4 Re^{-1.244}$ (IC2)$\zeta = 7.337 Re^{-0.33}$	±10%	Mitrovic and Peterson (2007) [22,24]
	●Water ●Monoethylene glycol ●Mixtures of water and Monoethylene glycol	Experimental	Blasius	$300 < Re < 10000$	Longitudinal ($s_R = 1.94$) Longitudinal ($s_R = 2$) Transversal ($s_R = 0.52$)	(IC3)$\zeta = 0.962 Re^{\frac{-1}{6.576}}$ (IC4)$\zeta = 1.351 Re^{\frac{-1}{7.710}}$ (IC5)$\zeta = 2.128 Re^{\frac{-1}{2.803}}$	±20%	Tran et al. (2015) [30,34]
	●Water	Numerical	Blasius	$1000 \leqslant Re \leqslant 8000$ $0.17 \leqslant s_{dia} \leqslant 0.24$ $0.071 \leqslant s_{inf} \leqslant 0.143$ $1000 \leqslant Re \leqslant 8000$ $0.17 \leqslant s_{dia} \leqslant 0.24$ $0.071 \leqslant s_{inf} \leqslant 0.143$ $1000 \leqslant Re \leqslant 8000$ $0.1 \leqslant s_{dia} \leqslant 0.14$ $0.042 \leqslant s_{inf} \leqslant 0.083$	Longitudinal ($s_{ratio} = 1.71$) Equidistant ($s_{ratio} = 1$) Transversal ($s_{ratio} = 0.58$)	(IC6) $\zeta = cRe^m$ $c = 1.35 s_{dia} + 2.8 s_{inf} + 0.92$ $m = 0.3 s_{dia} + 0.53 s_{inf} - 0.29$ (IC7) $\zeta = cRe^m$ $c = -15.3 s_{dia} + 1.4 s_{inf} + 5.4$ $m = 1.725 s_{dia} + 1.11 s_{inf} - 0.66$ (IC8) $\zeta = cRe^{-0.38}$ $c = 8.74 s_{dia} + 17 s_{inf} + 0.73$	±6%	Piper et al. (2017) [9]
	●Water	Numerical	Two-zone model based on Blasius	$1000 \leqslant Re \leqslant 8000$ $0.17 \leqslant s_{dia} \leqslant 0.24$ $0.071 \leqslant s_{inf} \leqslant 0.143$ $1000 \leqslant Re \leqslant 8000$ $0.17 \leqslant s_{dia} \leqslant 0.24$ $0.071 \leqslant s_{inf} \leqslant 0.143$ $1000 \leqslant Re \leqslant 8000$ $0.1 \leqslant s_{dia} \leqslant 0.14$ $0.042 \leqslant s_{inf} \leqslant 0.083$	Longitudinal ($s_{ratio} = 1.71$) Equidistant ($s_{ratio} = 1$) Transversal ($s_{ratio} = 0.58$)	(IC9)$\zeta_{MC} = (4.62 s_{inf} + 0.6) Re^{-0.34}$ (IC10)$\zeta_{MC} = (2.52 s_{inf} + 0.24) Re^{-0.3}$ (IC11)$\zeta_{MC} = (4.36 s_{inf} + 1.14) Re^{-0.44}$	NM	Piper et al. (2017) [9]
	●Water	Experimental	Churchill	$30 \leqslant Re \leqslant 8500$ $0.5 \leqslant s_R \leqslant 2$ $0.1 \leqslant \left(\frac{\delta}{s_{D,ws}}\right) \leqslant 0.2$	Any	(IC12)[#] $\zeta = 8\left[\left(\frac{12 + C_1}{Re}\right)^{12} + \frac{1}{(A+B)^{\frac{3}{2}}}\right]^{\frac{1}{12}}$ $A = \left[C_2 \ln\left(\frac{C_3}{\left(\frac{7C_4}{Re}\right)^{0.9} + 0.27 \times 10^{-5}}\right)\right]^{16}$ $B = \left[\frac{3.7530 C_5}{Re}\right]^{16}$ $C_1 = \left[2.171 s_r + 66.605\left(\frac{\delta}{s_{D.ws}}\right)\right]^{1.077} - 7.868$ $C_2 = \left[0.508 s_r + 7.169\left(\frac{\delta}{s_{D.ws}}\right)\right]^{-2.468} + 0.237$ $C_3 = \left[0.323 s_r + 2.646\left(\frac{\delta}{s_{D.ws}}\right)\right]^{14.03} + 4.59$ $C_4 = (1.239 s_r)^{-2.284} + 1.109\left(\frac{\delta}{s_{D.ws}}\right) - 0.188$ $C_5 = 1439 s_r^2 + 256900\left(\frac{\delta}{s_{D.ws}}\right)^2 - 38450\left(\frac{s_r \delta}{s_{D.ws}}\right) - 775.9$	±9%	Arsenyeva et al. (2018; 2019) [19,43,54]
Outer	●Isopropanol (two-phase)	Experimental	Custom power-law	$3000 \leqslant Re_{eq} \leqslant 9500$	Transversal	(OC1)[*] $\zeta = 0.01204 Re_{eq}^{-0.61705} Bo^{0.00728} Ka^{0.84292}$	±10%	Mitrovic and Peterson (2007) [23,24]
	●Water	Numerical	Blasius	$9500 \leqslant Re \leqslant 30000$	Longitudinal	(OC2)$\zeta = 2.187 Re^{-0.356}$	±1.5%	Piper et al. (2015) [33]
	●Water	Numerical	Blasius	$5000 \leqslant Re \leqslant 15000$	Longitudinal	(OC3)$\zeta = 3.46 Re^{-0.39}$	±2%	

(continued on next page)

Table 8 (*continued*)

Channel	HTF	Development	Format	Application[&]	Pattern	Correlation(s)	Deviation	Reference
								Piper et al. (2016) [37]
	●Dry air	Experimental	Blasius	$3000 \leqslant Re \leqslant 20000$	Mixed	(OC4)$\zeta = 0.7155 Re^{-0.361}$	±10%	Arsenyeva et al. (2018; 2019) [19,42,43,54]

[#] There is a typo in the original publication for the term *B*, where originally the multiplier was 37,530 but the results were found to be wrong.
[*] The equivalent Reynolds is defined using the equivalent mass flow rate in Equation (13) and liquid viscosity (μ_L).
[&] For s_{dia}, s_{inf}, $s_{D,ws}$ and s_R see Equations (2), (3), (7) and (8), respectively.

most correlations are developed for water, which can be used for comparison. Nevertheless, for a proper analysis, the pitch pattern was considered (often overlooked in literature). Fig. 11 shows variation of friction factor versus Reynolds with error bars showing the deviation. The legends show the pitch patten (L: longitudinal, T: transversal and M: mixed), geometrical characteristics, working fluid, correlation number (according to Table 8) and reference.

Regarding IC, for an apple-to-apple comparison, IC3/IC6/IC12 (from

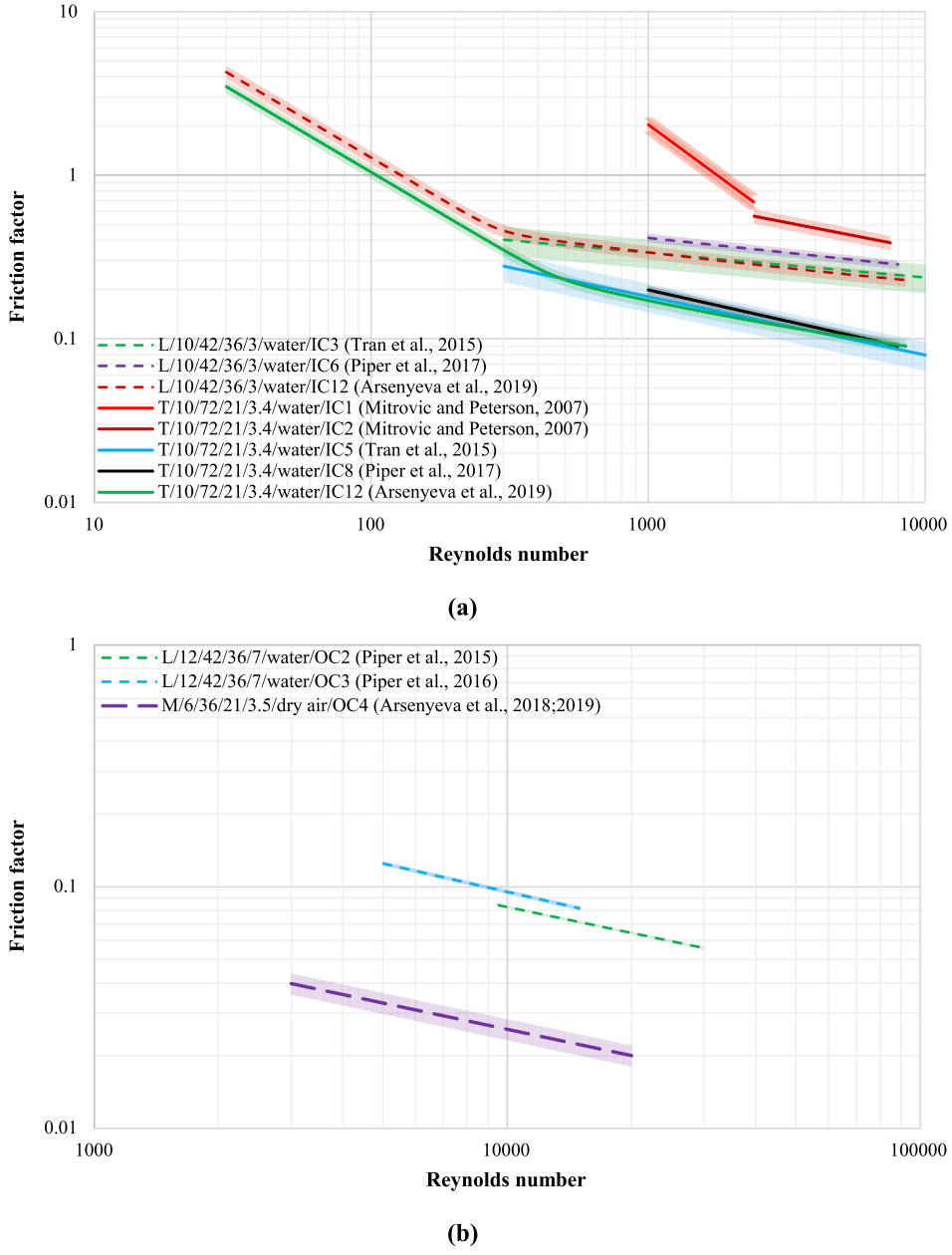

Fig. 11. Variation of friction factor versus Reynolds according to Table 8 for (a) inner channel and (b) outer channel.

Table 9
Chronological summary of the correlations developed for Nusselt.

Channel	HTF	Development	Format	Application/comment[&]	Pattern	Correlation(s)	Deviation	Reference
Inner	●Water ●Marlotherm oil (single-phase)	Experimental	Dittus and Boelter	$1000 \leqslant Re \leqslant 7500$	Transversal	(IC1) $Nu = 1.869 Re^{0.444} Pr^{-0.484}$	±10%	Mitrovic and Peterson (2007) [22,24]
	●Water	Numerical	Custom power-law	Application range: •$d_h = 2.5...8.4, 2s_L = 42, s_T = 72, L = 500, Re = 500...4000$ •$d_h = 3.8, 2s_L = 42, s_T = 40...100, L = 500, Re = 500...4000$ •$d_h = 3.8, 2s_L = 28...31, s_T = 72, L = 500, Re = 500...4000$	Varied	(IC2) [$] $Nu = 0.102\left(\frac{2s_L}{L}\right)^{0}\left(\frac{s_T}{2L}\right)^{-0.69}\left(\frac{d_h}{L}\right)^{0.66} Re^{0.6}$ Valid for water only while for other working fluids the constant (i.e., 0.102) should be replaced by: $c = 0.102\left(\frac{Pr}{Pr_w}\right)^{n}; Pr_w = 5.97, 0.33 < n < 0.45$ (the exponent n remained undetermined)	NM	Mitrovic and Maletic (2011) [26]
	●Water ●Monoethylene glycol ●Mixtures of water and monoethylene glycol	Experimental	Dittus and Boelter	$300 < Re < 10000$ $2 < Pr < 80$	Longitudinal ($s_R = 1.94$) Longitudinal ($s_R = 2$) Transversal ($s_R = 0.52$)	(IC3) $Nu = 0.057 Re^{0.752} Pr^{0.348}$ (IC4) $Nu = 0.067 Re^{0.774} Pr^{0.338}$ (IC5) $Nu = 0.065 Re^{0.699} Pr^{0.341}$	±20%	Tran et al. (2015) [30,34]
	●Water	Numerical	Dittus and Boelter	$1000 \leqslant Re \leqslant 8000$	Longitudinal	(IC6) $Nu \propto Re^{0.76} Pr^{0.38}$	NM	Piper et al. (2016) [20]
	●Water	Numerical	Dittus and Boelter	$1000 \leqslant Re \leqslant 8000$ $1 \leqslant Pr \leqslant 150$ $0.17 \leqslant s_{dia} \leqslant 0.24$ $0.071 \leqslant s_{inf} \leqslant 0.143$	Longitudinal ($s_{ratio} = 1.71$)	$Nu = cRe^m Pr^{0.4}$ (IC7) [&] $c = -0.163 s_{dia} + 0.711 s_{inf} + 0.022$ $m = 0.29 s_{dia} - s_{inf} + 0.8$	±15%	Piper et al. (2017) [9]
				$1000 \leqslant Re \leqslant 8000$ $1 \leqslant Pr \leqslant 150$ $0.17 \leqslant s_{dia} \leqslant 0.24$ $0.071 \leqslant s_{inf} \leqslant 0.143$	Equidistant ($s_{ratio} = 1$)	$Nu = cRe^m Pr^{0.4}$ (IC8) [&] $c = 0.03 s_{dia} + 0.76 s_{inf} - 0.032$ $m = -1.12 s_{inf} + 0.905$		
				$1000 \leqslant Re \leqslant 8000$ $1 \leqslant Pr \leqslant 150$ $0.1 \leqslant s_{dia} \leqslant 0.14$ $0.042 \leqslant s_{inf} \leqslant 0.083$	Transversal ($s_{ratio} = 0.58$)	$Nu = cRe^m Pr^{0.4}$ (IC9) [&] $c = 0.0775 s_{dia} + 0.38 s_{inf} + 0.005$ $m = 0.75$		
	●Water	Numerical	Two-zone model based on Petukhov	$1000 \leqslant Re \leqslant 8000$ $5 \leqslant Pr \leqslant 150$ Other conditions in Table 10	Longitudinal ($s_{ratio} = 1.71$) Equidistant ($s_{ratio} = 1$) Transversal ($s_{ratio} = 0.58$)	(IC10) See coefficients in Table 10 $Nu_{MC} = \frac{\left(\frac{\zeta_{MC}}{8}\right) Re_{MC} Pr}{1.07 + 12.7\sqrt{\left(\frac{\zeta_{MC}}{8}\right)}\left(Pr^{\frac{2}{3}} - 1\right)} \quad 5 \leqslant Pr \leqslant 150$ $Nu_{MC} = \frac{\left(\frac{\zeta_{MC}}{8}\right) Re_{MC} Pr}{1 + 3.4\zeta_{MC} + \left(11.7 + 1.8 Pr^{\frac{-1}{3}}\right)\sqrt{\left(\frac{\zeta_{MC}}{8}\right)}\left(Pr^{\frac{2}{3}} - 1\right)} \quad Pr < 5$	±15%	Piper et al. (2017) [9]
	●Water	Numerical	Blasius	$1200 \leqslant Re \leqslant 7800$ $0.5833 \leqslant s_{ratio} \leqslant 1$ $0.04167 \leqslant s_{dia} \leqslant 0.0833$ $0.083 \leqslant s_{inf} \leqslant 0.2381$	Transversal Equidistant	$Nu = cRe^m$ (IC11) $c = 2.178\left(-0.00194 s_{ratio} - 0.1496 s_{dia} + 0.00241 s_{inf} + 0.00286\right)$ $m = 1.635 s_{dia} + 0.0744 s_{inf} + 0.6969$	±10%	Kumar et al. (2019) [51]
Outer	●Isopropanol (two-phase)	Experimental	Custom power-law		Transversal		±10%	Mitrovic and

(*continued on next page*)

Table 9 (*continued*)

Channel	HTF	Development	Format	Application/comment[&]	Pattern	Correlation(s)	Deviation	Reference
				$10 < Re_{con} < 70$ $Re_{con} = \frac{u_{vap}\delta_f}{\nu_{liq}}$		(OC1)$Nu = 0.208\left(\frac{\theta}{\delta_N}\right)^{-0.5977} Pr_L^{0.45348}\left(\tau_w^*\right)^{0.98599} Ka^{0.03897}$ $\delta_N = \left(\frac{\nu_L^2}{g}Re_{con}\right)^{\frac{1}{3}}$ $\tau_W^* = \frac{\tau_W}{L_c(\rho_L - \rho_V)g}$ $L_c = \left(\frac{\rho_L}{\rho_L - \rho_V}\frac{\nu_L^2}{g}\right)^{\frac{1}{3}}$		Peterson (2007) [23,24]
	●Water	Numerical	Dittus and Boelter	$9500 \leqslant Re \leqslant 30000$ $6 \leqslant Pr \leqslant 150$	Longitudinal	(OC2)$Nu = 0.06Re^{0.745}Pr^{0.35}$	±2%	Piper et al. (2015) [33]
	●Water	Numerical	Generalized Lévêque equation (GLE)	$9500 \leqslant Re \leqslant 30000$ $6 \leqslant Pr \leqslant 150$	Longitudinal	(OC3)$Nu = 0.404\left(\frac{0.58\zeta Re^2 Prd_h}{s_L}\right)^{\frac{1}{3}}$	±30%	Piper et al. (2015) [33]
	●Water	Numerical	Petukhov	$9500 \leqslant Re \leqslant 30000$ $6 \leqslant Pr \leqslant 150$	Longitudinal	(OC4)$Nu = \frac{\left(\frac{0.58\zeta}{8}\right)RePr}{1.07 + 12.7\sqrt{\left(\frac{0.58\zeta}{8}\right)}\left(Pr^{\frac{2}{3}} - 1\right)}$	±5%	Piper et al. (2015) [33]
	●Water	Numerical	Dittus and Boelter	$5000 \leqslant Re \leqslant 15000$ Conducted only for $Pr = 6$ and the Pr exponent was assumed to be 1/3 (typical for turbulent forced convection)	Longitudinal	(OC5)$Nu = 0.091Re^{0.74}Pr^{\frac{1}{3}}$	±2%	Piper et al. (2016) [37]
	●Water ●Water glycerol mixture	Experimental	Dittus and Boelter	$450 \leqslant Re \leqslant 5800$ $1.7 \leqslant Pr \leqslant 3.8$	NM	(OC6)$Nu = 0.059Re^{0.71}Pr^{0.33}$	±20%	Goedecke and Scholl (2017–19) [45,49,81]
	●Dry air	Experimental	Dittus and Boelter	$2000 \leqslant Re \leqslant 20000$	Mixed	(OC7) $^*Nu = 2.187Re^{0.356}Pr^{0.4}$	±10%	Arsenyeva et al. (2018) [43]
	●Dry air	Experimental	Dittus and Boelter	$3000 \leqslant Re \leqslant 20000$	Mixed	(OC8)$Nu = 0.0275Re^{0.8175}Pr^{0.4}$	±10%	Arsenyeva et al. (2018; 2019) [19,42]

[&]Note that n was found to be a weak function of the mentioned parameters (i.e., n varying in the range 0.38…0.42) where an average value of 0.4 was found to result in only ± 5% deviation.

[$] There seems to be a typo in the original publication for the exponent of $2s_L/L$ in Nu correlation.

[*] There is a typo in the original publication in the exponent m which was mistakenly reported to be negative (i.e., −0.356).

[&] For s_{ratio}, s_{dia} and s_{inf} see Equations (1), (2) and (3), respectively.

Table 8) were used for a longitudinal PPHX design (10/42/36/3:$d_{ws}/s_T/2s_L/h_i$). Fig. 11a shows an agreement among the correlations but IC12 is recommended due to its general nature and less deviation. Similarly, a transversal design (10/72/21/3.4:$d_{ws}/s_T/2s_L/h_i$) was selected for IC1/IC2/IC5/IC8/IC12. According to Fig. 11a, IC1/IC2 behaved differently, and the overestimation is because inlet and outlet pressure drop values (by cross-sectional change) were not excluded from pressure loss calculations [34]. Moreover, the definition of geometrical properties for IC1/IC2 [22,24] were different, making a proper comparison impossible. Conversely, IC5/IC8/IC12 had a similar trend and again IC12 can be recommended due to the same advantages mentioned earlier.

Regarding OC, Fig. 11b shows the trend for OC2/OC3/OC4. The first two correlations are presented for longitudinal configuration using water (12/42/36/7:$d_{ws}/s_T/2s_L/h_i$), while the latter is for a mixed configuration using dry air (6/36/21/3.5:$d_{ws}/s_T/2s_L/h_i$). Unfortunately, they are insufficient for a general conclusion similar to IC. Again, it should be emphasized that OC1 should be used with caution (due to the pressure loss overestimation and different geometrical properties).

In summary, when using water, IC12 can be used to evaluate IC friction factor of all pitch patterns. A similar conclusion cannot be drawn for OC due to the lack of a general correlation. Therefore, further studies are required to investigate this and also other working fluids (e.g., refrigerants), especially under two-phase condition.

5.4.2. Nusselt number

Table 9 summarizes the Nusselt correlations where most correlations are in Dittus and Boelter format (see Equation (15)). The main limitation with constant c and m values is that they would be specific to a unique geometry (details in Table 1). In other words, for each PPHX geometry, a different correlation should be developed which is time consuming and technically inefficient [33]. Consequently, as shown in Table 9, other techniques can be used (e.g., two-zone models or analogy between heat and mass transfer).

As discussed in Section 5.3.1, in the two-zone model [9], two zones are considered within IC (i.e., for the recirculation zone and MC). As mentioned, MC accounts for the majority of heat transfer with fully-developed flow (thermally and hydrodynamically). Therefore, in the two-zone model, the MC was transformed into the corresponding pipe flow with the same hydraulic diameter as the MC. Consequently, specific Nusselt correlations were developed for MC (denoted by Nu_{MC}) in Petukhov format (IC10 in Table 9), as a function of Prandtl, friction factor in MC (IC9-11 in Table 8) and Reynolds in MC [9]:

$$Re_{MC} = Re\left(\frac{S^*}{1-\psi_A}\right) \tag{23}$$

where S^* and ψ_A are two dimensionless parameters (see Table 10). Once heat transfer coefficient in MC (h_{MC}) is determined, it is used to calculate the PPHX heat transfer coefficient [9]:

$$h = h_{MC}\left(\frac{1-\psi_A}{1-\psi_Q}\right) \tag{24}$$

with ψ_Q being another dimensionless parameter (see Table 10).

According to Table 9, for both channels, most correlations were developed for water, with more options for IC. For further analysis, a procedure similar to Section 5.4.1 is followed. Note that some studies did not report the pitch pattern and as such were excluded from the analysis. Fig. 12 shows Nusselt variation versus Reynolds for specific PPHX designs.

For IC, Fig. 12a compares the prediction of correlations for longitudinal and transversal pillow-plates (10/42/36/3 and 10/72/21/3.4:$d_{ws}/s_T/2s_L/h_i$, respectively). For the longitudinal pitch pattern, the predictions are hardly distinguishable and as such IC10 can be recommended due to its general nature. For the transversal pitch pattern, IC1 shows a different trend than the rest. As mentioned, this is due to the different geometrical properties definitions by Mitrovic and Peterson [22,24] compared to the other studies. Again, for transversal pitch pattern, IC10 can be recommended for Nusselt.

Fig. 12b illustrates variation of OC Nusselt for longitudinal and mixed PPHXs (12/42/36/7 and 6/36/21/3.5:$d_{ws}/s_T/2s_L/h_i$, respectively). Note that for a meaningful comparison, each category had a similar distance between the adjacent plates (13 mm and 12 mm for the longitudinal and mixed patterns, respectively). According to the figure, all the correlations for the longitudinal configuration had a similar trend but for some reason OC5 behaved differently. It can be mentioned that OC4 is a suitable option given its flexibilities. For the mixed pitch patten, the two correlations had different behaviors. It is unclear why this happened despite all the similarities between the two studies. Overall, only one correlation is available for transversal pattern (OC1, for which as mentioned, proper geometrical properties should be used). This indicates that more studies are needed to address this shortcoming.

Note that almost all these correlations were developed using constant wall temperature boundary condition (see Table 6). Zibart and Kenig [4] found this assumption equivalent to a fin efficiency of one over the WSs. Consequently, they treated each WS similar to multiple triangular fins with fin length of half WS diameter ($0.5d_{ws}$) and fin thickness equal to two plate thicknesses ($2\delta_p$) with the fin tips located at the center of the WS and fin efficiency as:

$$\eta_{ws} = \frac{\tanh\left(L_{fin}\sqrt{\frac{2h_{OC}}{k_P\delta_{fin}}}\right)}{L_{fin}\sqrt{\frac{2h_{OC}}{k_P\delta_{fin}}}} = \frac{\tanh\left(\frac{d_{ws}}{2}\sqrt{\frac{h_{OC}}{k_P\delta_P}}\right)}{\frac{d_{ws}}{2}\sqrt{\frac{h_{OC}}{k_P\delta_P}}} \tag{25}$$

Consequently, the specific thermal resistance in OC was defined as:

$$r_{OC} = \frac{1}{h_{OC}(1+\eta_{ws}\psi_{ws})} \tag{26}$$

where h_{OC} can be obtained from correlations in Table 9 and ψ_{ws} is defined in Equation (5). They also developed two corrective functions to modify the specific thermal resistance of plate (r_P) and that of IC (r_{IC}) [4]:

$$r_{P,corr} = f_P r_P = \left[\frac{1}{(1.11-0.79\delta_P^{-1.2}\eta_{ws})\left(\frac{h_{OC}}{h_{IC}}\right)^{0.01}}\right] r_P \tag{27}$$

Table 10
Coefficient values for the two-zone model developed by Piper et al. [9] (i.e., IC10 in Table 9).

Pitch pattern	Coefficient values				Conditions[&]
	ψ_A	ψ_Q	$d_{h,MC}$	S^*	
Longitudinal ($s_{ratio}=1.71$)	$0.81s_{dia}+0.263$	$0.46s_{dia}+1.17s_{inf}-0.042$	$-8.1s_{dia}+60s_{inf}+2.1$	1.0761	$0.17\leqslant s_{dia}\leqslant 0.24$ $0.071\leqslant s_{inf}\leqslant 0.143$
Equidistant ($s_{ratio}=1$)	$0.75s_{dia}+0.46$	$0.75s_{dia}+1.54s_{inf}-0.014$	$-18.31s_{dia}+35.42s_{inf}+4.8$	1	$0.17\leqslant s_{dia}\leqslant 0.24$ $0.071\leqslant s_{inf}\leqslant 0.143$
Transversal ($s_{ratio}=0.58$)	$0.94s_{dia}+0.4$	$2.16s_{dia}+4.23s_{inf}-0.0352$	$-11.22s_{dia}+113s_{inf}+1.82$	1	$0.1\leqslant s_{dia}\leqslant 0.14$ $0.042\leqslant s_{inf}\leqslant 0.083$

[&] For s_{dia} and s_{inf} see Equations (2) and (3), respectively.

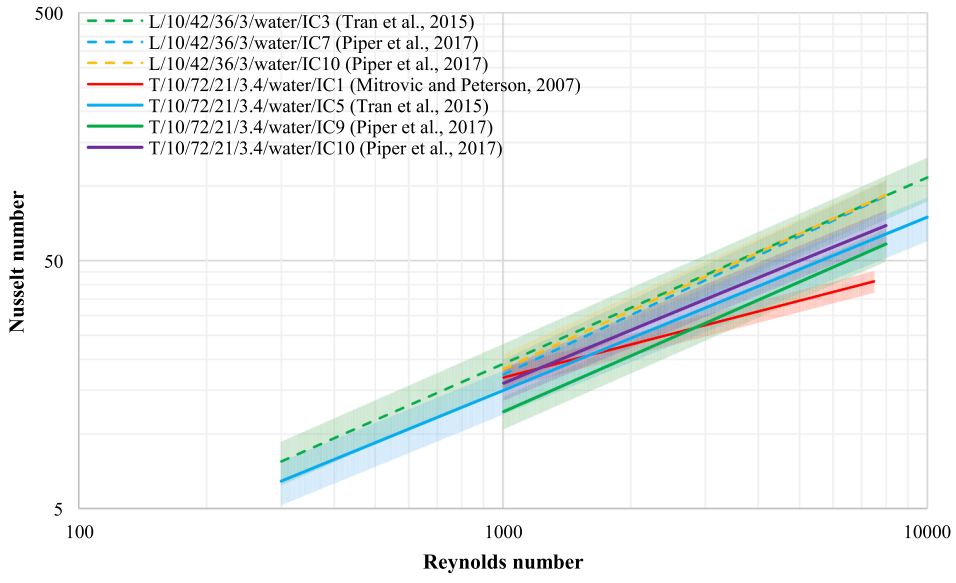

(a)

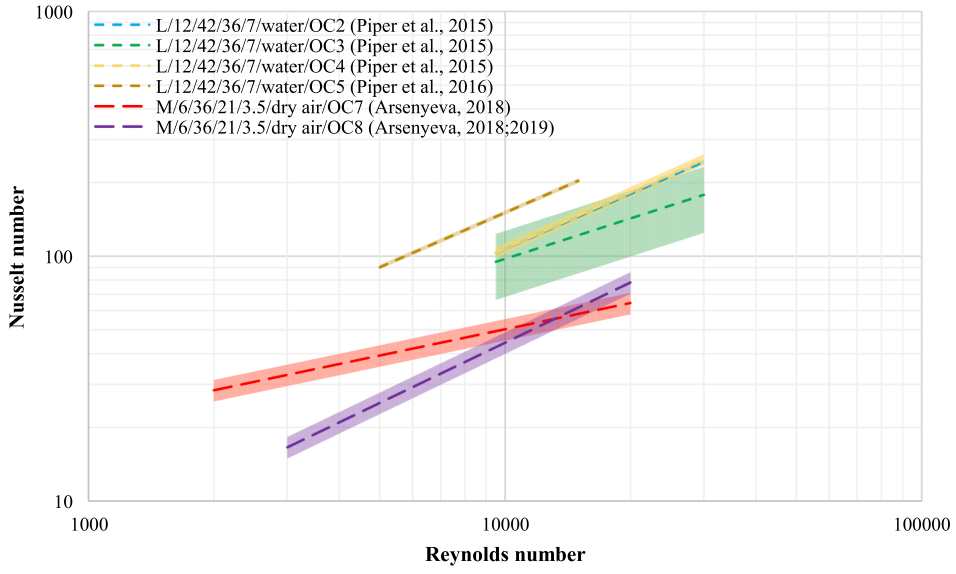

(b)

Fig. 12. Variation of Nusselt versus Reynolds according to Table 9 for (a) inner channel and (b) outer channel.

$$r_{IC,corr} = f_{IC} r_{IC} = \left[\frac{1}{(0.055\delta_P^{0.439}(\eta_{ws} - 1) + 1)\left(\frac{h_{OC}}{h_{IC}}\right)^{0.016}} \right] r_{IC} \tag{28}$$

Note that the corrective functions were developed under counter-current flow and their validity for other flow configurations is unknown. Besides, the plate material had an impact where WSs in OC were thermally almost unactive for SS (high thermal resistance), making constant wall temperature assumption invalid. For aluminum plates, however, the results were closer to those obtained with constant wall temperature [4].

In summary, IC10 can be used for water to evaluate Nusselt of different pitch patterns. For working fluids with strong temperature-dependent thermophysical properties within boundary layer, Sieder and Tate correlation was recommended for turbulent heat transfer [9]:

$$Nu_{Temp} = Nu\left(\frac{Pr}{Pr_W}\right)^{0.11} \tag{29}$$

where Pr and Pr_W are Prandtl numbers evaluated at the bulk and wall temperatures, respectively. Equation (24) had significant deviation, while Equation (29) presented under 2% deviation [9].

Overall, OC lacks a general correlation. Thus, more studies are needed on this topic and also to investigate other working fluids especially under two-phase conditions. Finally, although the mixed pitch patterns are not common, it is worth mentioning that no correlation has been developed for their IC heat transfer.

6. Investigated topics

6.1. Heat transfer enhancement

The effect of dimples on pillow-plate was numerically investigated

for OC flow [48]. Compared to smooth surface, the area was extended by about 1% while generating more but smaller and weaker recirculation zones. Overall, the dimpled PPHX had about 9% lower pressure drop but 2.2% higher heat transfer coefficient enhancing thermohydraulic efficiency (see Equation (20)) by about 11%. These were attributed to the changes in recirculation zones and relatively lower flow velocity in the dimpled pillow-plate due to its larger cross-sectional area. Note that dimples have only been investigated for pillow-plates with longitudinal pitch pattern, indicating that further research is required. Besides, corrugated pillow-plates can be another option for heat transfer enhancement [65].

6.2. Addition of nanoparticles

To enhance IC heat transfer, the effect of adding nanoparticles to water was numerically investigated where nanofluids with PEC (see Equation (22)) values above one can be considered as thermohydraulically justifiable.

Al-Turki et al. [64] investigated Al_2O_3 nanoparticles (concentrations and Reynolds of 0-3 vol% and 250–1000, respectively). In all cases, PEC was higher than one, where the highest nanoparticle concentration had the best performance. Similar results were reported by Shirzad et al. [52] who also investigated CuO and TiO_2 nanoparticles at different concentrations (0–5 vol%) under different Reynolds (1000–8000). CuO had the highest friction factor hence it was excluded from the list. At 2 vol%, Al_2O_3 had the highest PEC, whereas at 5 vol%, TiO_2 overtook Al_2O_3 for Reynolds above 2000. This is because higher concentrations enhanced the heat transfer coefficient but also friction factor. At higher Reynolds, the impact on friction factor was relatively constant, while heat transfer coefficient was highly influenced.

Overall, Al-Turki et al. [64] investigated a pillow-plate length of only $2s_L$ including the hydrodynamically developing region, while Shirzad et al. [52] considered what appears to be $10s_L$ and it seems the flow is fully-developed. As such the findings are not intercomparable. Note that nanofluids have not yet been investigated in OC.

6.3. Effect of weld-spot shape

Some studies investigated the impact of changing the WS shape. Note that in such studies the pitch pattern cannot be defined/determined according to Section 2.4.4. For instance, the effect of WS shape was investigated by comparing the performance of circular (with longitudinal pitch pattern) and elliptical shapes [5]. For the latter, the transversal and longitudinal diameters had the same size and twice the size of the circular shape, respectively. For such elliptical WSs, MC was found to suppress the recirculation zones, causing smaller recirculation. Consequently, the flow deflection and maximum velocity were lower. Overall, the heat transfer and pressure drop reductions were found to be 4% and 18%, respectively, thermohydraulically outperforming the circular shape. This was achieved despite that the pillow-plate with elliptical WSs had lower IC heat transfer surface area compared to circular WSs.

Later, the effect of WS shape was also investigated for elliptical shapes having the same surface area as circular ones [20]. In PPHXs originally having longitudinal pitch pattern, the utilization of elliptical shapes shrank the recirculation zones mainly due to the change in IC waviness as the separation point was not affected. For elliptical shapes, comparing the same diameter spots with those having the same area as circular ones, the latter had an improved thermohydraulic efficiency since the reduction in heat transfer coefficient was lower than the reduction of pressure losses. Conversely, for the transversal configuration no significant change in the flow pattern was observed when using elliptical shapes. Quantitatively, changing the WS shape from circular to streamlined oval (with the same area) enhanced the thermohydraulic efficiency by 37% and 22% for longitudinal and transversal pitch patterns, respectively.

In another series of studies by Eldeeb et al. [41,58], the WS shape was optimized (using approximation assisted optimization) to achieve the maximum thermohydraulic performance. The entire process of geometry generation, CFD analysis, metamodel development and optimization was automated as indicated in Fig. 13a. Briefly, first, design of experiment based on Latin hypercube sampling generated the parameterized designs. In this step, weld shapes were generated based on fourth-order nonuniform rational B-splines. After conducting CFD, a metamodel (based on Kriging method with quadratic global mean and spherical correlation) was developed. Finally, optimization was conducted based on multi-objective genetic algorithm. The results indicated that more streamlined and smaller shapes benefited from lower pressure drop due to the formation of smaller recirculation zones behind the WSs. Therefore, the optimum shapes were found to be more streamlined with width to height ratio (WHR) values within the range of 1.6–2 (i.e., almond as well as eye-shaped, see Fig. 13b). For the optimization, pitch ratio (s_{ratio}) values in the range of 0.58–1.73 ware considered, covering from transversal to longitudinal pitch pattern. The optimum pitch ratio values were within the range of 0.58–1.36. This is very important as it indicates that no optimal condition was found beyond a certain value (i.e., $s_{ratio} = 1.36$). Overall, the manufacturability and structural stability of such optimum shapes needs attention. Note that in these studies the shapes have been optimized/investigated only according to IC fluid flow and heat transfer. In other words, the effect of WS shape on the thermohydraulic behavior in OC has not yet been investigated.

6.4. Comparison with tube bundle

Performance of IC flow in a longitudinal PPHX was compared with a characteristically similar tube bundle (i.e., having the same cross-sectional area while their diameter was equal to the PPHX hydraulic diameter) [37]. The PPHX had superior performance at lower Reynolds in terms of thermohydraulic efficiency ratio (see Equation (21)). The reason is that for higher Reynolds, the pressure losses increase in PPHXs, deteriorating their performance. Consequently, under the same pumping power, PPHXs could not outperform the bundle beyond a certain Reynolds. A similar analysis was conducted for OC. For the same pumping power, the PPHX outperformed the bundle in the entire pumping power range. However, the PPHX underperformed for the same Reynolds.

A similar analysis was conducted for a transversal PPHX where its performance was compared with a characteristically similar tube bundle [12]. The results indicated that at lower Reynolds, the PPHX outperformed the tube bundle primarily due the stronger turbulence caused by WSs. However, as Reynolds increased the performance of the tube bundle improved or even exceeded that of the PPHX.

Overall, at lower Reynolds PPHXs are superior to characteristically similar tube bundles. Note that such comparison is currently missing for mixed and equidistant pitch patterns.

6.5. Comparison with other plate heat exchangers

In the literature, the performance of PPHXs has been compared with other PHXs (i.e., smooth, Chevron and Compabloc). In this section, a brief comparison is provided.

As mentioned, WSs disrupt the formation of boundary layer in PPHXs, creating flow resistance. Therefore, their pressure drop is higher than smooth PHXs [40]. In terms of heat transfer, higher temperatures were observed around WSs compared to smooth PHXs. This was attributed to the smaller local inflation in PPHXs [40].

Under similar operating conditions, the required heat transfer area for PPHXs is smaller than Chevron (by about 30% [19]) and Compabloc PHXs [50]. The main reason is that in PPHXs, the OC has the freedom in terms of distance.

When the hot and cold HTFs have equal flow rates, Chevron PHXs require less heat transfer surface area than PPHXs [50]. However, for unequal flow rates, PPHXs outperform Chevron PHXs. This is because

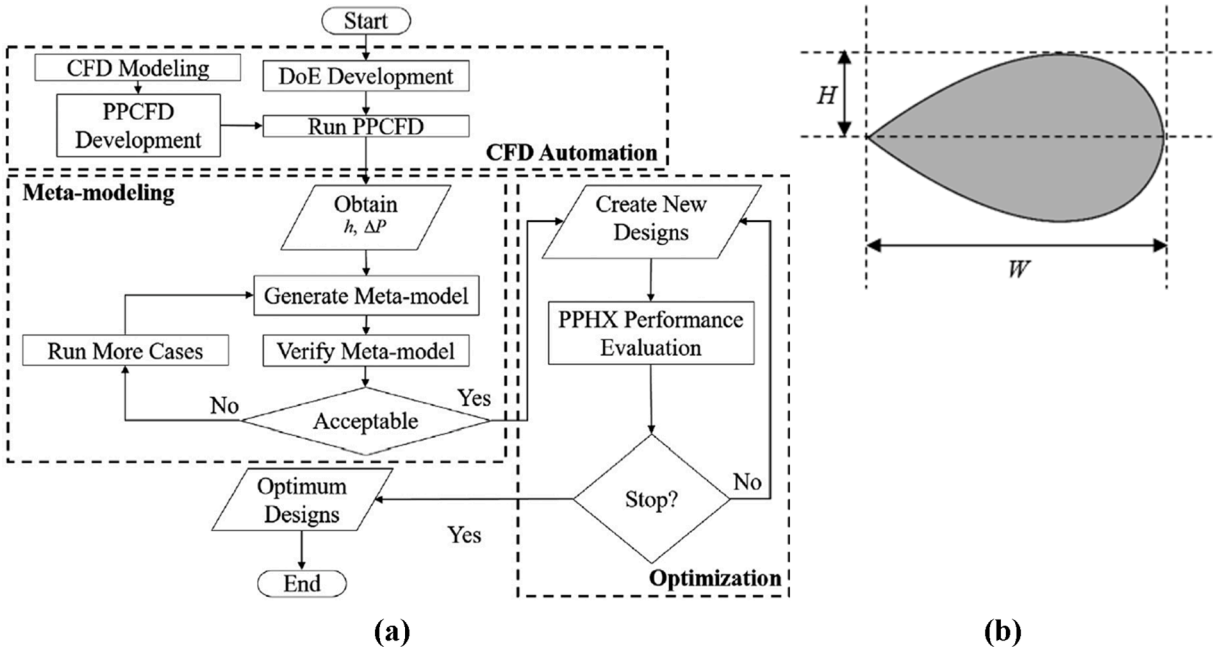

Fig. 13. (a) flowchart representation of the optimization procedure followed by Eldeeb et al. [41,58] (reprinted from International Journal of Refrigeration, 110, R. Eldeeb, V. Aute, R. Radermacher, Pillow plate heat exchanger weld shape optimization using approximation and parallel parameterized CFD and non-uniform rational B-splines, 121–131, Copyright (2020), with permission from Elsevier) and (b) definition of width to height ratio.

the latter would require multi-pass configuration, having higher pressure losses. Contrastingly, in PPHXs, the OC distance can be adjusted accordingly. Generally, PPHXs are recommended for cases where the flow rates differ significantly between the HTFs [19,50].

Under similar operating conditions, the pressure drop of the optimal non-circular PPHX (presented in Section 6.3) was found to be lower than (about a quarter of) a Chevron PHX; however, the heat transfer coefficient was slightly affected [58].

It is also worth mentioning the highest exergy loss under various Reynolds (turbulent regime) was found for Chevron PHXs followed by PPHXs and smooth PHXs which was attributed to the compact structure of Chevron PHXs as well as higher pressure loss due to the secondary flow [40].

7. Investigated applications

7.1. Condenser

Among first PPHX applications was its use in distillation columns as the top condenser where normally IC and OC host the cooling and process mediums, respectively [12]. Tran et al. [27] used two lab-scale setups and one pilot-scale plant to investigate the OC condensation of steam and chlorobenzene, respectively, in presence of noncondensables. They also studied the IC phenomena (using water) and found that the heat transfer coefficient was superior to a pipe with the same hydraulic diameter. Later, using experimental data from the same systems, they developed correlations for Nusselt and friction factor for IC using water, monoethylene glycol (MEG) and their mixtures [30,34] (see Section 5.4). Considering multiple correlations for analogous plain tube bundles (with the same hydraulic diameter and cross-sectional area as the investigated PPHXs), the IC heat transfer in PPHXs was found to be superior (even at low Reynolds); however, it came at higher pressure drop penalty [34]. They also reported the mean condensation heat transfer coefficient values under six operating conditions but fell short of developing correlations [30]. A summary of the findings with detailed explanation was reported by Tran et al. [12] including recommendations to enhance condensation in OC using baffles [82] or inserts [83]. Overall, characterization of condensation in PPHXs is not well-known yet and further experimental/numerical investigation is needed to fill this literature gap.

7.2. Evaporator/reboiler

PPHXs have been experimented as thermosyphon reboilers in distillation columns. In such application, the flow is density-driven and is termed as natural circulation evaporation (NCE) where subcooled liquid from the bottom of the distillation column enters the reboiler. As such, there are two zones in the reboiler, the sensible heating zone followed by the evaporation zone. Once evaporated, the low-density vapor flows back to the distillation column.

Goedecke and Scholl [29,31,35] experimentally investigated a thermosyphon reboiler where water or water-glycerol mixture was evaporated in OC by condensation of saturated steam in IC. Higher driving temperature difference was found to enhance the heat transfer and shorten the sensible heating zone. Consequently, the inlet velocity was increased but the magnitude of impact decreased at higher temperature differences, due to the higher pressure drop. Moreover, following a stepwise reduction in submergence it was found that down to a certain submergence the inlet velocity remained constant and then decreased, which was attributed to the increased hydrostatic pressure resulting in enhanced circulation driving force [31]. Overall, they reported that with PPHXs, the typical operating boundaries of tubular thermosyphon reboilers can be extended to lower operating pressures, lower driving temperature differences and lower submergence.

Tran et al. [39] combined the concept of PPHX condenser (see Section 7.1) with PPHX reboiler to evaporate the cooling medium in IC. To mimic condensation in OC, an electrical rectifier was used while R134a evaporated under thermosyphon (i.e., NCE) and forced circulation evaporation (FCE). Nucleate boiling was found to desirably be the dominant heat transfer mechanism even at lower heat fluxes and at lower temperature differences, unlike typical plateaus commonly observed for tubes due to the convective flow boiling. Besides, the two-phase heat transfer coefficient values under NCE were found to be higher in the PPHX than predictions from Kandlikar correlation [84] for an analogous vertical tube bundle with the same hydraulic diameter. This was mainly because in vertical tubes, the formed bubbles would be

entrained at the center of the tubes, moving upwards away from the walls. However, in PPHXs, the bubbles would be frequently deflected upon hitting the WSs, increasing the heat transfer intensity. Although definitive conclusions could not be made due to the relatively high uncertainty of Kandlikar correlation (about 20%), it was recommended for initial estimations. Nevertheless, the study fell short of confirming if the correlation can be applied for initial estimations under FCE.

Rekstad et al. [36,38] conducted demonstration studies on PPHXs as evaporator in RSW chiller units using CO_2 as the refrigerant in IC. Three setups were investigated to cool RSW to −1°C where the achieved subcooling was desirably within 3–4 °C. Nevertheless, they did not further investigate the refrigerant flow and heat transfer.

Overall, a detailed summary of the findings was compiled by Scholl [45]. PPHXs have shown promising performance as evaporators/reboilers; however, the scope of the investigations has been limited with no correlation development; thus, further studies are needed.

7.3. Falling film

Few studies investigated falling film on pillow-plate surfaces and the wetting/dewetting behavior. Such analyses have potential application in condensers or evaporators as well as ice production and as such a separate section has been dedicated to falling film.

In falling-film evaporators, a cuboid-shaped PPHX package is commonly placed within a cylindrical shell [45]. Consequently, when evaporation occurs in OC, the resulting vapor can freely move from the sides, resulting in lower pressure drop compared to falling-film STHXs. But the challenge is that a liquid distributor needs to be mounted atop each plate. For instance, trough-type distributors are frequently used in distillation towers [45].

Siebeneck et al. [15] experimentally investigated isothermal flow of deionized water (mixed with a fluorescent dye) over flat and pillow plates. It was found that for the same film Reynolds the film was thicker on pillow-plates with the difference growing as the film Reynolds increased. This was found to be due to the flow deceleration over the pillows resulting in higher film thickness. The following correlation was developed for the mean film thickness over pillow-plates:

$$\delta_f = 0.573\left(\frac{\nu_f^2}{g}\right)Re_f^{0.5175} \quad 0 \leqslant Re_f \leqslant 620 \tag{30}$$

Two types of flow were observed over pillow-plates: V-shaped towards each WS and inverse-V-shaped after WS (over the inflation). Piper et al. [32] reported similar findings and divided the flow into two zones, one with faster thicker film along the longitudinally-aligned WSs (Zone 1) and another in the remaining space with less speed and thickness (Zone 2), with widths of almost d_{ws} and $0.5s_T$–d_{ws}, respectively. The zones form even by the first top WS followed by a continuous drainage from Zone 2 to 1 until stabilization (regardless of film Reynolds). Using the same geometry, Zibart and Kenig [46] numerically investigated falling-film behavior in STAR-CCM+ (see Table 5) using the volume of fluid (VOF) method. There was an acceptable agreement between numerical and experimental results; however, the numerical film disturbance was produced later than the experiments. This could be due to the numerically ideal inlet condition, which is impossible in experiments since minor disturbances are unavoidable. Furthermore, there were unrealistic capillary waves in the numerical results and piecewise linear interface calculation method, currently available in ANSYS Fluent, was recommended.

Overall, aside from these qualitative analyses (further details in [45]), no correlation has been developed. Besides, although Siebeneck et al. [15] did not specify the investigated pitch pattern, from the figures it appears to be longitudinal. As such, further studies are needed for other pitch patterns as well as two-phase heat transfer.

7.4. Thermal energy storage

Selvnes et al. designed a cold thermal energy storage (CTES) unit using a PPHX [17]. The unit was coupled to the secondary circuit of a large-scale cascade refrigeration system for industrial applications where ammonia (R717) and CO_2 (R744) were used in the primary and secondary circuits, respectively. The system was expected to deliver cooling and freezing demands at −5°C and −40 °C, respectively. Due to the substantial difference between these two operating temperatures, CTES was considered for peak load shifting. Consequently, they designed a lab-scale prototype to conduct experiments using water as the phase change material (PCM). During the tests, the refrigerant (R744) circulated through the IC for condensation (or evaporation), while the PCM underwent melting (or solidification).

They also numerically studied two 2D sections of the CTES by cutting it transversally and longitudinally. In the former study [56], the impact of pillow-plate waviness was investigated by comparing with a flat plate heat exchanger. Natural convection was found to be stronger for the PPHX, especially at the beginning. Nevertheless, their phase change duration was similar, making future investigations simpler. Accordingly, in the latter study [55], the pillow-plate waviness was neglected and instead a flat plate was considered. The mushy zone constant (i.e., the measure for steepness of reaching zero velocity during solidification) was investigated for both melting and solidification indicating higher values prolonged the phase change duration.

Later, an experimental setup was constructed to investigate the impact of HTF inlet temperature, HTF mass flow rate and plate distance on the charging and discharging performance of the CTES unit in a CO_2 refrigeration system [60,63]. A smaller plate distance was found necessary for covering short but large peaks. Moreover, compared to the HTF mass flow rate, the HTF temperature was found to have a more significant impact on the average PCM discharge rate, especially at higher plate distances. Consequently, HTF temperature can be used to achieve a specific discharge rate to meet the cooling load profile for a specific application. Similar results were reported using a commercial organic PCM with phase change temperature around −9 °C [62,85]. Moreover, a temperature difference of about 5 °C between the PCM phase change temperature and HTF charging temperature was found as the best balance between heat transfer and energy consumption.

In 2020, Sevault and Næss [61] designed a thermal storage unit integrated with the central heating system of an office building to cover the peak heating demand. The organic PCM (phase change temperature of 35–37 °C) occupied OC, while water circulated in IC with two passes. A PPHX was favored (over fin-and-tube) due to its compactness while achieving higher heat output and durability. The storage capacity was 200 kWh with 3 tons of PCM, while using a water tank would have required about four times more volume. Previous dynamic simulations of their system showed that the unit could achieve heat input/output above 12 kW for more than 6 h using only 3–6 °C difference between the PCM phase change and HTF temperatures [86].

Sevault et al. [87] later built and implemented the PCM-PPHX unit and made several practical recommendations. They highlighted that one of the main cost drivers for PPHXs is the number of plates rather than their dimensions, due to their manufacturing process. It is thus more economical to maximize the size of each plate (within production constraints) and minimize the number of plates.

Also in 2020, Lin et al. [59] constructed a novel heat exchanger (see Fig. 14) for heat storage based on the concept of pillow-plates where IC was divided into two separate sections so that different HTFs can be used for charging and discharging. For both processes, the average power and effectiveness were found to decrease over time which was due to the decreasing temperature difference between the PCM and HTF [59]. Moreover, increasing the HTF flow rate enhanced the power (due to the stronger turbulence) while diminishing the effectiveness; nevertheless, beyond a certain flow rate the impact was negligible.

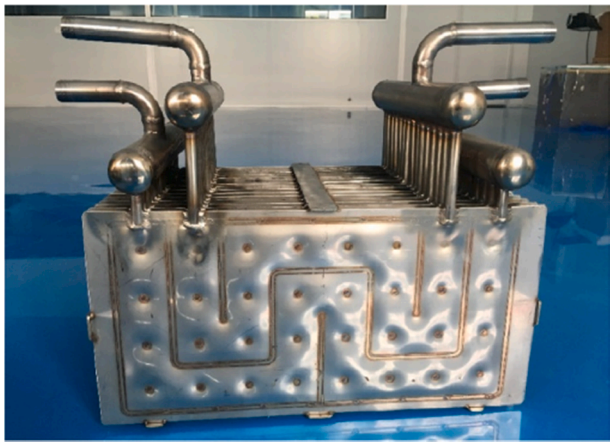

Fig. 14. Photographic view of the heat exchanger investigated by Lin et al. [59] (reprinted from Applied Thermal Engineering, 178, W. Lin, W. Zhang, Z. Ling, X. Fang, Z. Zhang, Experimental study of the thermal performance of a novel plate type heat exchanger with phase change material, 115630, Copyright (2020), with permission from Elsevier).

8. Concluding remarks

The main findings from the literature can be summarized as:

- A common framework for the terms used for geometrical design parameters is not established. There are examples where geometrical terms were used interchangeably or not reported in a standardized way, making the comparison of results challenging. The current work proposed a terminology to be followed in future studies.
- The number of studies, both numerical and experimental, are limited relative to other heat exchangers. Therefore, despite application and research for more than a decade, a reliable design tool is currently missing along with the common engineering knowledge.
- Given the high number of design parameters, comprehensive optimization studies are still needed to analyze their impact for both channels.
- The variety of investigated fluids in the inner and outer channels is limited, with water being the dominant to date. Experimental and numerical investigations on two-phase flow are scarce, possibly due to the already complicated flow behavior and complex geometry of the pillow-plate heat exchangers compared to tubes and conventional heat exchangers.
- The longitudinal pattern has received most attention in the literature, and the publications consistently reported its superior heat transfer performance to the transversal configuration. Although the transversal pattern could outperform longitudinal pattern under certain conditions when considering pressure drop, the characterization is most complete for the latter.
- Despite progress on friction factor and Nusselt correlations, heat transfer and fluid flow characteristics in the inner and outer channels have not been completely characterized. Nevertheless, the provided overview and suggestions can help readers select the appropriate correlations for the given configurations and conditions.
- The benefits of pillow-plate heat exchangers compared to their competitors are mainly its superior heat exchange efficiency, particularly at lower Reynolds. Compared with conventional Chevron plate heat exchangers, the flexibility in changing the outer channel distance allows up to 30% saving of heat exchanger area when the flow rate in outer and inner channels differ significantly.
- The reported applications are mainly as condensers and reboilers/evaporators in distillation columns for the process industry. However, there is a recent growing interest for thermal energy storage integrated into hydronic heating systems and refrigeration systems.
- An important missing component in the earlier studies is the cost. This is of great significance when it comes to selecting pillow-plate heat exchangers over their competitors.

9. Recommendations for future work

9.1. General

- **Flow configuration:** Crossflow needs further investigation for any potential benefits over the more commonly studied concurrent and counter-current flow configurations.
- **Heat transfer enhancement:** Investigating the heat transfer enhancement technique of adding dimples to the plates seems promising but have so far only been limited to longitudinal pitch pattern, indicating further research is required to fully understand its effect.
- **Material:** New plate materials should be of high interest, such as aluminum. This potentially enhances the heat transfer compared to stainless steel, the dominant material to date. Aluminum could also potentially reduce the cost and lower the carbon footprint.
- **Cost:** Currently a comprehensive comparative study on the capital and operating costs of pillow-plate heat exchangers compared to their competitors is missing.

9.2. Thermohydraulic

- **Friction factor and Nusselt correlations:** More studies are required to establish a representative friction factor correlation for the outer channel. For the inner channel, it would be of high interest to investigate other fluids than water.
- **Two-phase flow:** Overall, two-phase flow in pillow-plate heat exchangers is not well-characterized yet and further experimental and numerical investigation is needed.

9.3. Applications

- **Application as falling film heat exchanger:** The potential has been demonstrated based on mostly qualitative studies, but no general correlations were proposed, needing further research.
- **Application as evaporators/reboilers:** The scope of the investigations has been limited and correlations should be developed, needing further investigations.
- **Application as thermal storage:** despite some recent advancement on this frontier, further research is needed on design parameters including pitch pattern.

Declaration of Competing Interest

The authors declare that they have no known competing financial interests or personal relationships that could have appeared to influence the work reported in this paper.

Acknowledgements

This study was carried out through the research project KSP PCM-STORE (308847) supported by the Research Council of Norway and industrial partners. PCM-STORE aims at building knowledge on novel PCM technologies for low and medium temperature thermal energy storage systems.

References

[1] R. Eldeeb, J. Ling, V. Aute, R. Radermacher, Heat transfer enhancement using approximation assisted optimization for pillow plate heat exchangers. 17th International Refrigeration and Air Conditioning Conference, 2018.

[2] R. Eldeeb, V. Aute, R. Radermacher, Investigation of thermal-hydraulic characteristics of pillow plate heat exchangers using CFD. 16th International Refrigeration and Air Conditioning Conference, 2016.
[3] B. Maletić, Modelling and Numerical Simulation of Fluid Flow and Heat Transfer in Thermoplates, University of Paderborn, Paderborn, Germany, 2009.
[4] A. Zibart, E. Kenig, Numerical investigation of conjugate heat transfer in a pillow-plate heat exchanger, Int. J. Heat Mass Transf. 165 (2021), 120567.
[5] M. Piper, A. Zibart, J.M. Tran, E.Y. Kenig, A numerical study on turbulent single-phase flow and heat transfer in pillow plates. 15th International Heat Transfer Conference, 2014.
[6] J.M. Tran, M. Piper, E.Y. Kenig, S. Scholl, Pillow-plate heat exchangers: Fundamental characteristics, in: Innovative Heat Exchangers, Springer, 2018, pp. 233–245.
[7] J. Mitrovic, B. Maletic, Numerical simulation of fluid flow, heat transfer and pressure drop in thermoplates, in: HEFAT 2007, 2007.
[8] R.I. Håvard, E.T.M.J. Sigmund, Dimple plate heat exchangers for a sea-water chiller using CO_2 as refrigerant, design and testing, in: 24th IIR International Congress of Refrigeration, Yokohama, Japan, August 16–22, 2015, 2015.
[9] M. Piper, A. Zibart, E. Kenig, New design equations for turbulent forced convection heat transfer and pressure loss in pillow-plate channels, Int. J. Therm. Sci. 120 (2017) 459–468.
[10] A.E. Rosenblad, Method of forming dimpled plate heat exchanger elements by the use of hydrostatic pressure, in, Google Patents, 1970.
[11] A. Peze, Welded plate fin heat exchanger and heat exchanger plate fin manufacturing process, in, 1996.
[12] J.M. Tran, M. Piper, E.Y. Kenig, Single-phase flow and condensation in pillow-plate condensers, in, in: H.-J. Bart, S. Scholl (Eds.), Innovative Heat Exchangers, Springer International Publishing, Cham, 2018, pp. 247–265.
[13] E. Djakow, R. Springer, W. Homberg, M. Piper, J. Tran, A. Zibart, E. Kenig, Incremental electrohydraulic forming-A new approach for the manufacture of structured multifunctional sheet metal blanks, in: AIP Conference Proceedings, vol. 1896, AIP Publishing LLC, 2017, pp. 080003.
[14] M. Vocciante, E.Y. Kenig, Pillow-plate heat exchangers: an overview on advances, limitations and prospects, Chem. Eng. Trans. 88 (2021) 865–870.
[15] K. Siebeneck, W. Popov, T. Stefanak, S. Scholl, Pillow plate heat exchangers–Investigation of flow characteristics and wetting behavior at single-flow conditions, Chem. Ing. Tech. 87 (2015) 235–243.
[16] O. Arsenyeva, P. Kapustenko, O. Vasilenko, J. Tran, E. Kenig, The estimation of heat transfer area of pillow-plate heat exchangers for water heating, 2017.
[17] H. Selvnes, A. Hafner, H. Kauko, Design of a cold thermal energy storage unit for industrial applications using CO_2 as refrigerant. 25th IIR International Congress of Refrigeration Proceedings, 2019.
[18] M. Piper, A. Olenberg, J. Tran, E. Kenig, Determination of the geometric design parameters of pillow-plate heat exchangers, Appl. Therm. Eng. 91 (2015) 1168–1175.
[19] O. Arsenyeva, M. Piper, A. Zibart, A. Olenberg, E.Y. Kenig, Investigation of heat transfer and hydraulic resistance in small-scale pillow-plate heat exchangers, Energy 181 (2019) 1213–1224.
[20] M. Piper, A. Zibart, J. Tran, E. Kenig, Numerical investigation of turbulent forced convection heat transfer in pillow plates, Int. J. Heat Mass Transf. 94 (2016) 516–527.
[21] J. Mitrovic, B. Maletic, Numerical simulation of fluid flow and heat transfer in thermoplates, in: International Heat Transfer Conference 13, Begel House Inc., 2006.
[22] J. Mitrovic, R. Peterson, Study of single-phase convection and condensation in thermoplate heat exchanger (part I), in: HEFAT 2007, 2007.
[23] J. Mitrovic, R. Peterson, Study of single-phase convection and condensation in thermoplate heat exchanger (part II), in: HEFAT 2007, 2007.
[24] J. Mitrovic, R. Peterson, Vapor condensation heat transfer in a thermoplate heat exchanger, Chem. Eng. Technol. 30 (2007) 907–919.
[25] B. Maletic, J. Mitrovic, Influence of the thermoplate geometry on the heat transfer. Proceedings of the 5th European Thermal-Sciences Conference EUROTHERM, 2008.
[26] J. Mitrovic, B. Maletic, Numerical simulation of fluid flow and heat transfer in thermoplates, Chem. Eng. Technol. 34 (9) (2011) 1439–1448.
[27] J. Tran, S. Sommerfeld, M. Piper, E. Kenig, Investigation of pillow-plate condensers for the application in distillation columns, in: 10th International Conference on Distillation and Absorption, Friedrichshafen, Germany, 2014, pp. 607–612.
[28] M. Piper, A. Olenberg, J. Tran, R. Goedecke, S. Scholl, E. Kenig, Bestimmung charakteristischer geometrieparameter von thermoblech-wärmeübertragern, Chem. Ing. Tech. 86 (8) (2014) 1214–1222.
[29] R. Goedecke, S. Scholl, Enlarged operation ranges for thermosiphon reboilers using thermoplates, in: 10th International Conference on Distillation and Absorption, Friedrichshafen, Germany, 2014, pp. 63–68.
[30] J. Tran, S. Sommerfeld, M. Piper, E. Kenig, Investigation of pillow-plate condensers for the application in distillation columns, Chem. Eng. Res. Des. 99 (2015) 67–74.
[31] R. Goedecke, S. Scholl, Enlarged operation ranges for thermosiphon reboilers using pillow plates, Chem. Eng. Res. Des. 99 (2015) 58–66.
[32] M. Piper, C. Wecker, A. Olenberg, J. Tran, E. Kenig, An experimental analysis of the topology and dynamics of a falling liquid film over the wavy surface of a vertical pillow plate, Chem. Eng. Sci. 130 (2015) 129–134.
[33] M. Piper, J.M. Tran, E.Y. Kenig, CFD-untersuchung der fluiddynamik und des wärmeübergangs bei einphasiger strömung im welligen spalt zwischen thermoblechen, Chem. Ing. Tech. 3 (2015) 216–225.
[34] J.M. Tran, M. Piper, E.Y. Kenig, Experimentelle untersuchung des konvektiven wärmeübergangs und druckverlustes in einphasig durchströmten thermoblechen, Chem. Ing. Tech. 3 (2015) 226–234.
[35] R. Goedecke, S. Scholl, Experimentelle untersuchung eines thermoblechapparates als naturumlaufverdampfer, Chem. Ing. Tech. 3 (2015) 244–252.
[36] I.H. Rekstad, T.M. Eikevik, S. Jenssen, Dimple plate heat exchangers for a sea-water chiller using CO_2 as refrigerant, design and testing, in: 24th IIR International Congress of Refrigeration, Yokohama, Japan, 2015.
[37] M. Piper, J.M. Tran, E.Y. Kenig, A CFD study of the thermo-hydraulic characteristics of pillow-plate heat exchangers. ASME 2016 Heat Transfer Summer Conference, American Society of Mechanical Engineers, Washington, DC, USA, 2016.
[38] I.H. Rekstad, Y. Ladam, Evaluation of different evaporator and condenser concepts in sea water chillers using CO_2 as refrigerant, in: 12th IIR Gustav Lorentzen Conference on Natural Refrigerants (GL2016), Edinbourg, United Kingdom, 2016.
[39] J. Tran, M. Linnemann, M. Piper, E. Kenig, On the coupled condensation-evaporation in pillow-plate condensers: Investigation of cooling medium evaporation, Appl. Therm. Eng. 124 (2017) 1471–1480.
[40] C. Zhang, D. Wang, Y. Han, Y. Zhu, X. Peng, Experimental and numerical investigation on the exergy and entransy performance of a novel plate heat exchanger, Exp. Heat Transfer 30 (2017) 162–177.
[41] R. Eldeeb, J. Ling, V. Aute, R. Radermacher, Weld shape optimization for pillow plate heat exchangers. 17th International Refrigeration and Air Conditioning Conference, 2018.
[42] O.P. Arsenyeva, M. Piper, A. Zibart, A. Olenberg, E.Y. Kenig, Heat transfer and pressure loss in small-scale pillow-plate heat exchangers, Chem. Eng. Trans. 70 (2018) 799–804.
[43] O. Arsenyeva, J. Tran, E.Y. Kenig, Thermal and hydraulic performance of pillow-plate heat exchangers, in: 28th European Symposium on Computer Aided Process Engineering, vol. 43, Elsevier, 2018, pp. 181–186.
[44] M. Vocciante, M. Piper, A. Zibart, E.Y. Kenig, Numerical evaluation of different turbulence models for single-phase flow in the outer pillow-plate channel, in: Computer Aided Chemical Engineering, vol. 43, Elsevier, 2018, pp. 397–402.
[45] S. Scholl, Pillow plate heat exchangers as falling film evaporator or thermosiphon reboiler, in: Innovative Heat Exchangers, Springer, 2018, pp. 267–294.
[46] A. Zibart, E.Y. Kenig, Falling liquid film flow over the wavy surface of vertical pillow plates - A numerical investigation. International Heat Transfer Conference Digital Library, Begel House Inc., 2018.
[47] S. Kumar, B. Premachandran, P. Subbarao, Numerical simulation of fluid flow and heat transfer in a pillow plate channel, in: International Heat Transfer Conference Digital Library, Begel House Inc., 2018.
[48] M. Piper, A. Zibart, E. Djakow, R. Springer, W. Homberg, E. Kenig, Heat transfer enhancement in pillow-plate heat exchangers with dimpled surfaces: A numerical study, Appl. Therm. Eng. 153 (2019) 142–146.
[49] R. Goedecke, S. Scholl, Modelling and simulation of a pillow plate thermosiphon reboiler, Heat Mass Transf. 55 (2019) 95–104.
[50] O. Arsenyeva, J. Tran, M. Piper, E. Kenig, An approach for pillow plate heat exchangers design for single-phase applications, Appl. Therm. Eng. 147 (2019) 579–591.
[51] S. Kumar, B. Premachandran, P. Subbarao, Study on thermo–hydraulics in a pillow plate channel, Int. J. Therm. Sci. 145 (2019), 106020.
[52] M. Shirzad, S.S.M. Ajarostaghi, M.A. Delavar, K. Sedighi, Improve the thermal performance of the pillow plate heat exchanger by using nanofluid: Numerical simulation, Adv. Powder Technol. 30 (2019) 1356–1365.
[53] M. Shirzad, M.A. Delavar, S.S.M. Ajarostaghi, K. Sedighi, Evaluation the effects of geometrical parameters on the performance of pillow plate heat exchanger, Chem. Eng. Res. Des. 150 (2019) 74–83.
[54] O. Arsenyeva, The hydraulic resistance in the small-scale pillow-plate heat exchangers, in: 2nd International Scientific Conference “Chemical Technology and Engineering”, Lviv, Ukraine, 2019.
[55] H. Selvnes, Y. Allouche, A. Sevault, A. Hafner, CFD modeling of ice formation and melting in horizontally cooled and heated plates, in: Eurotherm Seminar# 112-Advances in Thermal Energy Storage, Edicions de la Universitat de Lleida Lleida, Spain, 2019.
[56] H. Selvnes, Y. Allouche, A. Sevault, A. Hafner, A CFD analysis for the performance assessment of a novel design of plates-in-tank latent storage unit for freezing applications, in: 8th Conference on Ammonia and CO_2 Refrigeration Technologies, Proceedings, IIR, 2019.
[57] S. Kumar, B. Premachandran, P. Subbarao, Large eddy simulation of single-phase forced convection in pillow plate channel with periodic boundary conditions, Int. J. Heat Mass Transf. 149 (2020), 119176.
[58] R. Eldeeb, V. Aute, R. Radermacher, Pillow plate heat exchanger weld shape optimization using approximation and parallel parameterized CFD and non-uniform rational B-splines, Int. J. Refrig 110 (2020) 121–131.
[59] W. Lin, W. Zhang, Z. Ling, X. Fang, Z. Zhang, Experimental study of the thermal performance of a novel plate type heat exchanger with phase change material, Appl. Therm. Eng. 178 (2020), 115630.
[60] H. Selvnes, Y. Allouche, A. Sevault, A. Hafner, A CFD analysis for the performance assessment of a novel design of plates-in-tank latent storage unit for freezing applications, in: 8th Conference on Ammonia and CO_2 Refrigeration Technologies, Proceedings, IIR, 2019.
[61] H. Selvnes, Y. Allouche, A. Sevault, A. Hafner, A CFD analysis for the performance assessment of a novel design of plates-in-tank latent storage unit for freezing applications, in: 8th Conference on Ammonia and CO_2 Refrigeration Technologies, Proceedings, IIR, 2019.

[62] H. Selvnes, Y. Allouche, A. Hafner, A cold thermal energy storage unit for CO_2 refrigeration using phase change material: First experimental results, in: 9th Conference on Ammonia and CO_2 Refrigeration Technologies Ohrid, R. Macedonia September 16-17, 2021 Proceedings, International Institute of Refrigeration, 2021.
[63] H. Selvnes, Y. Allouche, A. Hafner, Experimental characterisation of a cold thermal energy storage unit with a pillow-plate heat exchanger design, Appl. Therm. Eng. 199 (2021), 117507.
[64] Y.A. Al-Turki, A. Yarmohammadi, A.a. Alizadeh, D. Toghraie,, Numerical investigation of nanofluid flow and heat transfer in a pillow plate heat exchanger using a two-phase model: Effects of the shape of the welding points used in the pillow plate, ZAMM-J. Appl. Math. Mech./Zeitschrift für Angewandte Mathematik und Mechanik (2021).
[65] Y. Guo, C. Qiu, M. Xu, W. Zhang, X. Yan, L. Li, Crack failure analysis of laser 316L stainless steel edge joints in pillow plate heat exchanger used in oil refinery, Eng. Fail. Anal. 122 (2021), 105215.
[66] Abaqus, in, Vol. 2021, Dassault Systèmes, https://www.3ds.com/products-services/simulia/products/abaqus/.
[67] M. Wolfshtein, The velocity and temperature distribution in one-dimensional flow with turbulence augmentation and pressure gradient, Int. J. Heat Mass Transf. 12 (1969) 301–318.
[68] T.-H. Shih, W.W. Liou, A. Shabbir, Z. Yang, J. Zhu, A new k-ϵ eddy viscosity model for high reynolds number turbulent flows, Comput. Fluids 24 (1995) 227–238.
[69] V. Yakhot, S. Orszag, S. Thangam, T. Gatski, C. Speziale, Development of turbulence models for shear flows by a double expansion technique, Physics of Fluids A, Fluid Dyn. 4 (1992) 1510–1520.
[70] P. Spalart, S. Allmaras, A one-equation turbulence model for aerodynamic flows, in: 30th aerospace sciences meeting and exhibit, 1992, pp. 439.
[71] F.-S. Lien, M. Leschziner, A pressure-velocity solution strategy for compressible flow and its application to shock/boundary-layer interaction using second-moment turbulence closure, J. Fluids Eng. 115 (1993) 717–725.
[72] D.K. Walters, D. Cokljat, A three-equation eddy-viscosity model for Reynolds-averaged Navier-Stokes simulations of transitional flow, J. Fluids Eng. 130 (2008), 121401.
[73] F.R. Menter, Two-equation eddy-viscosity turbulence models for engineering applications, AIAA J. 32 (1994) 1598–1605.
[74] F.R. Menter, M. Kuntz, R. Langtry, Ten years of industrial experience with the SST turbulence model, Turbulence, Heat Mass Transfer 4 (2003) 625–632.
[75] J. Smagorinsky, General circulation experiments with the primitive equations: I. The basic experiment, Monthly Weather Rev. 91 (1963) 99–164.
[76] F. Nicoud, F. Ducros, Subgrid-scale stress modelling based on the square of the velocity gradient tensor, Flow, Turbulence Combus. 62 (1999) 183–200.
[77] F. Dittus, L. Boelter, Heat transfer in automobile radiators of the tubular type, Int. Commun. Heat Mass Transfer 12 (1985) 3–22.
[78] B. Petukhov, Heat transfer and friction in turbulent pipe flow with variable physical properties, in: Advances in heat transfer, vol. 6, Elsevier, 1970, pp. 503–564.
[79] H. Martin, A theoretical approach to predict the performance of chevron-type plate heat exchangers, Chem. Eng. Process. Process Intensif. 35 (1996) 301–310.
[80] D.L. Gee, R. Webb, Forced convection heat transfer in helically rib-roughened tubes, Int. J. Heat Mass Transf. 23 (1980) 1127–1136.
[81] R. Goedecke, Naturumlaufverdampfung in Einem Kissenplattenapparat, Cuvillier Verlag, 2017.
[82] M. Piper, E. Kenig, Kissenplatten-Wärmeübertrager, in: D.D.P.-u. Markenamt (Ed.), Universitaet Paderborn, Germany, 2016.
[83] J. Tran, E. Kenig, Kissenplatten-Wärmeübertrager, in: D.D.P.-u. Markenamt (Ed.), Universitaet Paderborn, Germany, 2015.
[84] S.G. Kandlikar, A general correlation for saturated two-phase flow boiling heat transfer inside horizontal and vertical tubes, 1990.
[85] H. Selvnes, Y. Allouche, A. Hafner, C. Schlemminger, I. Tolstorebrov, Cold thermal energy storage for industrial CO_2 refrigeration systems using phase change material: An experimental study, Appl. Therm. Eng. 118543 (2022).
[86] A. Sevault, F. Bøhmer, E. Næss, L. Wang, Latent heat storage for centralized heating system in a ZEB living laboratory: integration and design, in: IOP Conference Series: Earth and Environmental Science, Vol. 352, IOP Publishing, 2019, pp. 012042.
[87] A. Sevault, F. Vullum-Bruer, O.L. Tranås, Active PCM-Based Thermal Energy Storage in Buildings, in: 14th Gustav Lorentzen Conference, Kyoto, Japan, December –9, 2020, 2020.